Nucleic Acids Research, 2024, **52**, 3971–3988
https://doi.org/10.1093/nar/gkae046
Advance access publication date: 1 February 2024
RNA and RNA-protein complexes

RAVER1 hinders lethal EMT and modulates miR/RISC activity by the control of alternative splicing

Alice Wedler[1,†], Nadine Bley[1,†], Markus Glaß[1], Simon Müller[1,2,3], Alexander Rausch[1], Marcell Lederer[1], Julia Urbainski[1], Laura Schian[1], Kingsley-Benjamin Obika[1], Theresa Simon[1], Lara Meret Peters[1], Claudia Misiak[1], Tommy Fuchs[1], Marcel Köhn[1], Roland Jacob[1], Tony Gutschner[1], Christian Ihling[4], Andrea Sinz[4] and Stefan Hüttelmaier[1,*]

[1]Institute of Molecular Medicine, Section for Molecular Cell Biology, Faculty of Medicine, Martin Luther University Halle-Wittenberg, 06120 Halle (Saale), Germany
[2]New York Genome Center, New York, NY, USA
[3]Department of Biology, New York University, New York, NY, USA
[4]Department of Pharmaceutical Chemistry and Bioanalytics, Institute of Pharmacy, Martin Luther University Halle-Wittenberg, 06120 Halle (Saale), Germany

[*]To whom correspondence should be addressed. Tel: +49 345 5573959; Fax: +49 345 5527126; Email: stefan.huettelmaier@medizin.uni-halle.de
[†]The first two authors should be regarded as Joint First Authors.

Abstract

The RAVER1 protein serves as a co-factor in guiding the polypyrimidine tract-binding protein (PTBP)-dependent control of alternative splicing (AS). Whether RAVER1 solely acts in concert with PTBPs and how it affects cancer cell fate remained elusive. Here, we provide the first comprehensive investigation of RAVER1-controlled AS in cancer cell models. This reveals a pro-oncogenic role of RAVER1 in modulating tumor growth and epithelial-mesenchymal-transition (EMT). Splicing analyses and protein-association studies indicate that RAVER1 guides AS in association with other splicing regulators, including PTBPs and SRSFs. In cancer cells, one major function of RAVER1 is the stimulation of proliferation and restriction of apoptosis. This involves the modulation of AS events within the miR/RISC pathway. Disturbance of RAVER1 impairs miR/RISC activity resulting in severely deregulated gene expression, which promotes lethal TGFB-driven EMT. Among others, RAVER1-modulated splicing events affect the insertion of protein interaction modules in factors guiding miR/RISC-dependent gene silencing. Most prominently, in all three human TNRC6 proteins, RAVER1 controls AS of GW-enriched motifs, which are essential for AGO2-binding and the formation of active miR/RISC complexes. We propose, that RAVER1 is a key modulator of AS events in the miR/RISC pathway ensuring proper abundance and composition of miR/RISC effectors. This ensures balanced expression of TGFB signaling effectors and limits TGFB induced lethal EMT.

Graphical abstract

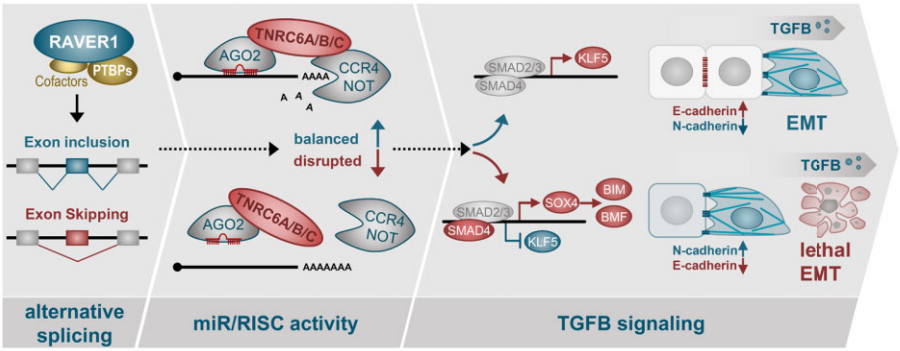

Introduction

The proper control of splicing, in particular alternative splicing (AS), is central for development and tissue homeostasis by guiding the synthesis of transcript variants ensuring protein isoform diversity (1). In cancer, splicing is largely deregulated due to mutation or aberrant expression of key splicing regulatory proteins (2,3). Previous studies have highlighted the polypyrimidine tract binding protein family (PTBPs) and associated proteins to serve central roles in the control of AS (4). PTBP1 represses or activates AS via CU-rich motifs (4–6). Association with such motifs via its four RNA recognition motifs (RRMs), oligomerization and the formation of

Received: June 15, 2023. **Revised:** December 24, 2023. **Editorial Decision:** January 9, 2024. **Accepted:** January 12, 2024

ternary complexes with co-factors was proposed to modulate PTBP-dependent splicing by RNA looping (7,8). Positional rules guiding this PTBP-dependent modulation of splicing were recently demonstrated by a capture RIC-seq (CRIC-seq) method, which enriches RBP-associated RNA-RNA fragments (9).

PTBP-modulated control of AS is frequently disturbed in cancer and deregulated expression of PTBPs is associated with adverse disease outcome in various malignancies (10–12). Elevated expression of PTBP1, the most abundant PTBP paralogue in most cancers, is associated with poor outcome in various solid cancers and clinical properties suggesting roles of PTBPs in cancer progression (12). In agreement, PTBPs have been reported to influence key signaling pathways, e.g. EGFR-, MAPK-, PI3K-signalling, although the molecular mechanisms underlying these regulatory roles remain partially elusive and likely vary in a cancer type-dependent manner (10). A prominent example of PTBP1-dependent control of cancer cell phenotypes is the modulation of a pro-glycolytic shift by PTBP1-dependent enhancement of pyruvate kinase PKM2 and down tuning of PKM1 (13).

Other RNA binding proteins (RBPs) impact on PTBP expression and function (10). The abundance of PTBP1 is controlled in part by nonsense-mediated decay (NMD) regulation, which essentially involves inclusion or skipping of exon 11 in *PTBP1* (14,15). ESPR1 promotes the inclusion of exon 11 leading to increased expression of PTBP1, whereas PTBP1 itself promotes skipping of this exon allowing balanced expression of PTBP1 by negative feed-back control. PTBP-dependent regulation of other splicing events, e.g. AS of tropomyosin (TPM1/2) (16), involves the interaction with other RBPs like RAVER1 (17). This protein was proposed to allow the tethering of distinct PTBPs assembled on the same pre-mRNA at distal and proximal regulatory sites of AS exons to foster out-looping (18). Next to three well-structured N-terminal RNA Recognition Motifs (RRMs), RAVER1 encompasses an extended intrinsically disordered region (IDR), which comprises up to four PTBP-interacting peptide motifs (19,20). These appear essential for the assembly of PTBP-RAVER complexes to direct AS and potentially also promote the association of both proteins in membrane-less protein-RNA condensates in the vicinity of nucleoli, termed perinucleolar compartments (PNC, (17,21)). Intriguingly, PNC size and frequency were proposed to indicate progressed cancer stages and were found associated with adverse disease outcome in cancer (21–23). However, if RAVER1 serves roles in cancer, PNC homeostasis and how this is interconnected with the potentially PTBP-dependent control of splicing in cancer progression remained essentially elusive.

This study presents the first examination of RAVER1's role in cancer cells, including a comprehensive investigation of RAVER1 modulated alternative splicing (AS). We demonstrate that RAVER1 serves partly PTBP1-independent pro-oncogenic roles impacting the balance of proliferation, apoptosis and EMT. In lung adenocarcinoma (LUAD) cells, RAVER1 hinders lethal, TGFB-driven EMT. This regulation is associated with RAVER1's role in the modulation of AS and overall miR/RISC activity. RAVER1 depletion and loss disturb AS resulting in deregulated abundance and composition of miR/RISC pathway effectors shifting miR/RISC activity. Our studies provide strong evidence that this deregulation essentially contributes to elevated lethal, TGFB-driven EMT in cancer cells. These findings suggest that RAVER1 promotes cancer progression by guiding AS and pro-oncogenic miR/RISC activity.

Materials and methods

Plasmids and cloning

Plasmid generation including vectors, respective templates and restrictions sites were summarized in Supplementary Table TS1. All constructs were validated by sequencing.

Cell culture, transfection, and transduction

A549, ES-2, Hep-G2, C-643, PANC-1 cells and HEK293T17 were cultured in DMEM (Gibco), H1650 and H522 cells were cultured in RPMI 1640 (Gibco) and BE(2)-C were cultured in a 1:1 mixture of DMEM/F12 (with HEPES, Gibco) and EMEM (ATCC), all supplemented with 10% FBS and incubated at 37° C with 5% CO_2. The origin of cancer cell lines is summarized in Supplementary Table TS2.

Cells were transfected with siRNA pools (72 h) and/or plasmids (Supplementary Table TS1) using Lipofectamine RNAiMax or Lipofectamine 3000 (Thermo Fisher Scientific) according to the manufacturer's instructions. Where indicated, cells were transferred to new culture plates 24 h post-transfection.

For lentivirus production, HEK293T17 cells were co-transfected with the packaging plasmids psPax2, pMD2.G and indicated lentiviral pLVX vectors, co-expressing iRFP or GFP as tracers, respectively. Lentiviral supernatant was collected 24–48 h post-transfection. Viral titers were determined 72 h post-infection of HEK293T17 cells and determined by flow cytometry (iRFP or GFP) using a MACS Quant Analyzer (Miltenyi BioTech). For lentiviral transduction cells were infected at 10 MOI (multiplicity of infection) for 72 h.

CRISPR/Cas9 knockout

For CRISPR/Cas9 mediated RAVER1 knockout 5×10^5 A549 cells were transfected with two sgRNA encoding plasmids (psg_RFP_RAVER1_Ex1 and psg_RFP_RAVER1_Ex8) and a Cas9 nuclease encoding plasmid (pcDNA-Cas9-T2A-GFP). RFP-/GFP-positive cells were isolated as single cell clones by FACS (Melody sorter, BD Bioscience) 48 h post-transfection. Knockout in populations derived from single cell clones was evaluated by Western blotting.

Cell proliferation, spheroid growth and anoikis resistance

Analyses of 2D cell proliferation, 3D spheroid growth and anoikis resistance were essentially performed as recently described (24). In brief, for knockdown studies, cells were transfected as indicated. Post-transfection (24 h), 1×10^3 cells were seeded per well in 96 well plates for 2D proliferation studies. Cell proliferation was analyzed 5 days post-seeding using bright field microscopy in an IncuCyte® S3 (Sartorius) device. For 3D spheroid growth and anoikis resistance studies, 1×10^3 cells were seeded per well – where indicated 24h post-transfection. For spheroid analyses, cells were centrifuged for 3 min at 300 g in Corning® 96 Well Clear Round Bottom Ultra Low Attachment microplates. Endpoint spheroid size was determined 5 days post-seeding by bright field microscopy using an IncuCyte® S3 (Sartorius) device. For anoikis resistance studies, cells were cultured at reduced FBS (1%) in Corning®

96 Well Clear Flat Bottom Ultra Low Attachment microplates. Cells were transferred to a round-bottom plate 5 days post-seeding, centrifuged for 3 min at 300 g to document cell clusters by brightfield microscopy in an Incucyte® S3 device. In addition, cell viability was determined for all 2D and 3D analyses using CellTiter-Glo® (Promega) according to the manufacturer's protocol. Cell viability was determined relative to the median of respective controls. In all studies, biological triplicates with at least three technical replicates were analyzed.

Caspase 3/7 activity

Caspase 3/7 activity was determined using CaspaseGlo 3/7 (Promega) according to manufacturer's protocols. In brief, 1×10^3 cells – where indicated 24 h post-transfection – were seeded per well in 96 well plates. Caspase 3/7 activity and cell viability (see above) were determined 5 days post-seeding if not indicated otherwise. Relative (rel.) apoptosis was determined by normalizing caspase 3/7 activity to cell viability and is shown relative to the median of control populations. In all studies, biological triplicates with at least three technical replicates were analyzed.

Wound closure migration assay

For determining cell migration by wound closure analyses, cells were seeded in 96-well Image lock microplates (Sartorius). Scratches were inserted in cell layers 24 h post-seeding using the Incucyte® S3 scratch maker module (Sartorius). Wound closure was monitored using brightfield microscopy (Incucyte® S3) and determined relative to control conditions, essentially as described previously (25).

Cell cycle analyses

Cell cycle progression was analyzed 72 h post-transfection of siRNA pools using propidium iodide staining and flow cytometry (MACSQuant Analyzer, Miltenyi Biotech), as recently described in (26).

RNA isolation and RT-PCR

Total RNA from cell lines was isolated using TRIzol. RNA concentration was determined using a NanoQuant plate (Tecan Spark), and RNA integrity was monitored on a Bioanalyzer 2100 (Agilent). For cDNA synthesis, 2 μg of total RNA served as a template using M-MLV Reverse Transcriptase (Promega) and random hexamer primers following manufacturer's protocol. Semi-quantitative PCR was performed using OneTaq DNA polymerase (NEB) and gene-specific primers (Supplementary table TS3) according to the manufacturer's protocol. PCR products were separated on 2% agarose gel containing ethidium bromide and documented using an E-Box Gel imager (Vilber). Quantitative PCR analyses were performed using the ORA™ qPCR Green ROX L Mix (HighQu) with indicated gene-specific primers (Supplementary table TS3) in a Roche LightCycler 480 II, as previously described (26).

Northern blot

Northern Blot analyses of microRNA expression were performed as previously described (27). Utilized probes are summarized in Supplementary table TS4.

Affinity-/immunopurification

For affinity purification of SBP/FLAG-tagged RAVER1 constructs, cleared cell lysates (1×10^7 cells per condition) using SBP-AP buffer (150 mM KCl, 50 mM Tris-pH 7.5, 5% (v/v) glycerol, 5 mM EDTA-pH 8, 0.25% (v/v) NP-40, 100 μg/ml digitonin) were incubated with MyOne streptavidin beads (Life Technologies) for 2 h at 4°C. After three washing steps with SBP-AP buffer, proteins were eluted by addition of NuPage LDS sample buffer (Thermo Fisher Scientific) supplemented with 50 mM DTT and incubation at 65°C for 5 min. Eluted proteins were analyzed by Western blotting or LC–MS/MS Analysis (see below). For the latter, samples were washed and heat-eluted with SBP-AP-MS-buffer (150 mM KCl, 50 mM Tris-pH 7.5, 5% (v/v) glycerol, 5 mM EDTA-pH 8, 0.1% (v/v) DDM). For co-immunoprecipitation of GFP-AGO2 and HA-tagged TNRC6B mutants, cells were extracted with Co-IP buffer (150 mM NaCl, 20 mM Tris-pH 7.5, 1 mM EDTA-pH 8, 0.5% (v/v) Triton X-100). Cleared cell lysates were incubated with GFP-antibodies and Protein G Dynabeads (Life Technologies), essentially as described above.

Identification of RAVER1 associated proteins by LC–MS/MS

Pulldown samples (three replicates; see immunoprecipitation above) were prepared for liquid chromatography/tandem mass spectrometry (LC–MS/MS) following a modified FASP (filter-aided sample preparation) protocol (28). Briefly, protein samples were incubated and washed with 8 M urea in 50 mM HEPES (4-(2-hydroxyethyl)-1-piperazineethanesulfonic acid), 10 mM TCEP, pH 8.5. Washing steps were performed using 0.5 mL centrifugal filter units (30-kDa cutoff, Sigma Aldrich, Darmstadt, Germany) and two centrifugation steps (14 000 × *g*, 10 min). Afterwards, alkylation of proteins was performed with 50 mM iodoacetamide in 8 M urea, 50 mM HEPES, pH 8.5 at room temperature (20 min in the dark). Samples were washed twice with 50 mM HEPES, pH 8.5 (18 000 × *g*, 2 × 10 min) before they were incubated with 1 μg trypsin in 50 mM HEPES, pH 8.5 at 37°C overnight. After enzymatic digestion, samples were acidified with trifluoro acetic acid (TFA) at 0.5% (v/v) final concentration.

Peptide solutions were analyzed by (LC–MS/MS) on an Ultimate 3000 RSLC nano-HPLC system coupled to a Q-Exactive Plus mass spectrometer with a Nanospray Flex ion source (all from Thermo Fisher Scientific). Samples were loaded onto an RP C18 pre-column (Acclaim PepMap, 300 μm × 5 mm, 5 μm, 100 Å, Thermo Fisher Scientific) and washed with 0.1% (*v*/*v*) TFA for 15 min at 30 μl/min. Peptides were eluted from the pre-column and separated on a 200 cm μPAC C18 separation column (Pharmafluidics) that had been equilibrated with 3% solvent B (solvent A: 0.1% (*v*/*v*) FA (formic acid), solvent B: ACN, 0.1% (*v*/*v*) FA). A linear gradient from 3–35% solvent B within 180 min at 600 nL/min (0–30 min) and 300 nl/min (30–180 min) was used to elute peptides from the separation column. Data were acquired in data-dependent MS/MS mode, HCD (higher-energy collision-induced dissociation) with a normalized collision energy (NCE) of 28% was used for fragmentation. Each high-resolution full MS scan (m/z 375 to 1799, $R = 140\,000$, target value (TV) 3 000 000, max. injection time (IT) 50 ms) was followed by high-resolution ($R = 17500$, TV 200 000, IT 120 ms, isolation window 2 Th) product ion scans, starting with

the most intense signal in the full scan MS, dynamic exclusion (duration 30 s, window ± 3 ppm) was enabled.

For peptide identification and quantification, data were searched against the Swiss-Prot database (tax. *Homo sapiens*, version 11/19; 20 315 entries) using Proteome Discoverer, version 2.4 (Thermo Fisher Scientific). A maximum mass deviation of 10 ppm was applied for precursor ions, while for product ions, max. 0.02 Da were allowed. Oxidation of Met and acetylation of protein N-termini were set as variable modifications. Carbamidomethylation of cysteines was included as fixed modification. A maximum of two missed cleavage sites were considered for peptides. Peptides were quantified via LFQ (label-free quantitation) and data were finally subjected to quantile normalization to derive protein enrichment by RAVER1.

Western blot

Protein expression was analyzed by Western blotting as previously described (29). Primary antibodies and fluorophore-coupled secondary antibodies are indicated in Supplementary table TS5.

TGFB treatment and lethal EMT analysis

Where indicated, cells were treated with TGF-β (TGFB). To this end, cells were seeded into 96-well plates 24 h post-transfection of siRNA where indicated. Cell numbers were adjusted to altered growth rates. Post-seeding (24 h), cells were treated for 72 h with 10 ng/ml recombinant human TGF-β1 (HEK293 derived, PEPROTECH). Cell density was monitored by an Incucyte S3 (Sartorius) and analyzed using the AI Cell Health Analysis Software (v2022B) to visualized TGFB-dependent changes. In addition, relative apoptosis was determined by evaluating caspase 3/7 activity and cell viability, essentially as described above.

Luciferase assay

Luciferase activity was analyzed 72 h post-transfection of luciferase-encoding reporters using DualGlo (Promega), essentially as previously described (26). Firefly luciferase (FFL) activities were normalized by Renilla (RL) activities yielding relative activities (RLU). RLU ratios were normalized to control populations and the luciferase empty vector control.

Immunostaining

Immunostainings were performed, essentially as previously described (29), using protein-specific antibodies summarized in Supplementary table TS5, Phalloidin-TRITC (Sigma) and DAPI (Sigma). Images were acquired using a SP8X confocal microscope (Leica) equipped with a white light laser and HyD detectors using standard settings for sequential acquisition. Images were quantified using Fiji (version 1.54d). For PNC quantifications the NuclearParticleDetector2D (MiToBo Cell Image Analyzer) within Fiji was used with a minimum region size of 10 pixels, essentially as previously described (30). PNC and nuclei masks were utilized to determine mean fluorescence intensities (MFI) for indicated proteins. To assess PNC intensities, the MFI of the respective nucleus was subtracted to account for distinct expression levels in individual cells. Intensity profiles determined by the 'plot profile' function using a straight line were averaged upon centering the structure of interest (PNCs or cell–cell contacts). To quantify changes in the localization of CDH2 and CTNNB1, MFI ratios of the contacts sides over the cytoplasm were evaluated (29). To determine cell-cell contact distribution and asses the percentage of cell-cell borders covered by cell-cell contacts, the 'plot profile' function was used to derive CTNNB1 fluorescence intensities. Representative CTNNB1 fluorescence profiles are shown. Cell-cell contacts were defined as CTNNB1 intensities above a threshold of 75.

RNA sequencing and data processing

PolyA mRNA sequencing of three independent analyses of controls, RAVER1- and PTBP1-depleted A549 cells was performed 72h post siRNA transfection. Strand-specific paired-end RNA sequencing was conducted by Novogene (Hong Kong) using Illumina NovaSeq 6000, resulting in 150 bp long reads with an average of 2 × 28 million reads per sample.

Quality of the raw fastq files was assessed using FastQC (https://www.bioinformatics.babraham.ac.uk/projects/fastqc/). Sequencing adapters and low quality read ends were clipped off using Cutadapt v2.8. The processed sequencing reads were aligned to the human genome (UCSC hg38) using HiSat2 v2.1.0. Alignments in the obtained bam files were sorted, indexed and secondary alignments were filtered out using samtools v1.10. FeatureCounts v2.0.0 was used for summarizing gene-mapped reads. Ensembl (GRCh38.100) was used as annotation basis. Differential gene expression was determined using the R package edgeR v3.38.4 utilizing trimmed mean of M-values normalization. A false discovery rate (FDR) adjusted p-value below 0.05 was considered significant for differential gene expression. For these analyses previously reported standard pipelines were used (26).

Differential isoform expression was quantified using rMATS turbo v4.1.2 (31) using the prior generated alignment files and Gencode v29 annotations (32). Protein-coding genes were determined using the R package biomaRt v.2.56.0, as previously described (26). Sashimi plots were generated using ggsashimi v1.1.5 (33) and Gencode v29 annotations. The PSI (precent spliced in) value determines the IncLevel derived from rMATS analyses.

Hexamer frequencies within significant ($|\Delta PSI| > 0.05$, FDR < 0.05) AS exons determined by RAVER1 and PTBP1 depletion were derived via genomic coordinates of spliced exons obtained from rMATS analyses (SE.MATS.JCEC.txt). These were extracted from determined skipped exon events in protein-coding genes identified by the R-package biomaRt, using ENSEMBL v100. Exon cDNA sequences were extracted from these coordinates using bedtools getfasta (34) and the UCSC hg38 human reference genome. cDNA sequences with lengths below the 5th and above the 95th percentile were removed and hexamer frequencies of the remaining sequences were determined via the R-package Biostrings v2.68.1. Absolute hexamer frequencies were divided by the total number of hexamers in all sequences to obtain normalized hexamer frequencies.

The enrichment of RBP binding motifs within significant AS exons were revealed by using the memes R-package utilizing the MEME suite (35). Shuffled input sequences with preserved di-nucleotide frequencies were used as background sequences. Ray2013_rbp_Homo_sapiens.dna_encoded.meme obtained from the MEME website (https://meme-suite.org/meme/) was applied as motif database.

Identification of hexamers mostly abundant in skipped exon sequences, was based on an enrichment frequency above 9e-4. Motifs were converted by the R-package Biostrings and matched against a database of RBP motifs (Ray2013_rbp_Homo_sapiens.dna_encoded.meme from https://meme-suite.org/meme/) using the runTomTom function of the memes R-package utilizing the MEME suite.

Gene set enrichment analyses

Gene set enrichment analyses (GSEA) was performed with the GSEA Software (version 4.2.3) and MsigDB gene sets (v2023.1) using the $\log_2$ fold change of mRNA expression, as derived from RNAseq, or the $\log_2$ fold enrichment of proteins with RAVER1, as determined by mass spectrometry, for ranking. Data were analyzed using the classic scoring mode and a minimal threshold of 10–15 genes for enrichment in specific sets, respectively.

Gene ontology analyses were performed using the R package clusterProfiler v4.8.1. The enrichment of the protein-coding genes with unique splicing events (FDR < 0.05, $|\Delta PSI| > 0.05$) in the MsigDB ontology gene set (v2023.1) was calculated and filtered for molecular functions – only enrichment with an FDR < 0.05 is shown.

Animal handling and ethics approvals

Immunodeficient athymic nude mice (FOXN1nu/nu) were obtained from Charles River (Wilmington, MA). Animals were handled according to the guidelines of the Martin Luther University based on ARRIVE guidelines. Permission was granted by the County Administration Office for Animal Care Saxony-Anhalt (42502-2-1625 MLU). iRFP-labelled (stably transduced) parental or RAVER1 depleted A549 cells (1×10^6) were harvested in PBS with 50% (v/v) Matrigel (Sigma) and were injected subcutaneously (sc) into 6-week-old female nude mice (6 mice per condition). Tumor growth of isoflurane-anaesthetized mice was monitored weekly by near-infrared imaging using a Pearl imager (LI-COR, Lincoln, NE) and quantified using the Image Studio software (LI-COR). Mice were sacrificed after 25 days when parental A549 tumors reached termination criteria. Tumor volume was calculated using the formula volume $V = \pi/6 \times L1 \times L2 \times L3$, essentially as previously described (36).

Kaplan–Meier and gene expression analyses

Hazardous ratios (HRs) for indicated genes were determined by the Kaplan–Meier (KM) plotter online tool using mRNA gene chip data for lung cancer, selected for 'best cutoff analyses and adenocarcinoma (www.kmplot.com). Survival data of the whole TCGA tumor cohort ($n = 33$) were performed by the Gene Expression Profiling Interactive Analysis (GEPIA) online tool (www.gepia2.cancer-pku.cn). Normalized primary tumor expression (FPKM) and associated clinical data derived from the TCGA (Cancer Genome Atlas Research Network, 2017) were obtained via the GDC data portal.

Structure prediction and biogrid analyses

For prediction and visualization of the RAVER1 protein structure (E9PAU2) AlphaFold DB (37) and PyMOL Molecular Graphics System (version 2.0, Schrödinger LLC) were used. Analysis of protein association with RAVER1 (E9PAU2) was performed using BioGRID webtool version 4.4.220 (https://thebiogrid.org/).

Results

RAVER1 promotes tumor cell proliferation

Pan-cancer analyses based on RNAseq data provided for 33 cancers via the TCGA suggested that upregulated expression of RAVER1 as well as PTBP1 is associated with unfavorable prognosis in various cancers (Figure 1A, B). Moreover, both proteins showed strongly, pan-cancer associated expression (Supplementary Figure S1A). In lung adenocarcinoma (LUAD), this trend was pronounced and the expression of both, RAVER1 and PTBP1, was significantly elevated. Notably, the median expression of splicing regulators is elevated in LUAD, although the expression of some splicing regulators, including RAVER2, is decreased. Intriguingly, however, survival analyses of the same splicing regulators in LUAD revealed that among PTBPs, only PTBP1 and even more strikingly RAVER1 show hazard ratios greater one (Supplementary Figure S1A; Supplementary Table TS14). These findings suggested that PTBP1, potentially in concert with RAVER1, serves conserved pro-oncogenic roles and that their elevated expression is associated with poor disease outcome.

This was investigated by loss-of-function studies in a panel of carcinoma- and neuroblastoma-derived (NBL) cell lines (Supplementary Table TS2). The depletion of RAVER1, using two independent siRNA pools, revealed consistent and significant downregulation of 2D tumor cell proliferation (Figure 1C; Supplementary Figure S1B). In contrast, growth rates were only modestly, in ES-2 cells even non-significantly, affected by the depletion of PTBP1. However, the only mild consequence of PTBP1 depletion might be due to partial compensation by upregulated PTBP2 expression (Supplementary Figure S1C). Moreover, the transient depletion of RAVER1 slightly decreased PTBP1 expression in some cell models and vice versa (Figure 1C; Supplementary Figure S1C). In contrast to depletion studies, the overexpression of GFP-RAVER1 in A549 (4.6-fold) did not reveal substantial disturbance of cell proliferation (Supplementary Figure S1D). Analyses in 3D cultures of three tumor cell lines (A549, ES-2 and HepG2) demonstrated that the depletion of RAVER1 significantly reduced spheroid growth and anoikis resistance, suggesting that RAVER1 is a conserved enhancer of tumor cell proliferation (Figure 1D, E; Supplementary Figure S1E, F). In agreement with 2D cell proliferation, PTBP1 depletion revealed non-consistent and only barely significant effects on spheroid growth and anoikis resistance (Supplementary Figure S1E, F). Whether RAVER1 or PTBP1 influence cell cycle progression was evaluated in A549, ES-2 and HepG2 cells in which depletion resulted in reduced proliferation. In all these cell models and independent of used siRNA pools, RAVER1 knockdown led to the significant, but modest enrichment of cells in the G1 and reduction in the S phase, suggesting slightly disturbed G1/S progression and DNA replication (Figure 1F; Supplementary Figure S1G–I). More strikingly, RAVER1 downregulation robustly elevated caspase 3/7 activity, suggesting the induction of apoptosis by RAVER1 downregulation (Figure 1G). Taken together, this supported a conserved, pro-proliferative and anti-apoptotic role of RAVER1 in cancer cells, which appeared less pronounced for PTBP1.

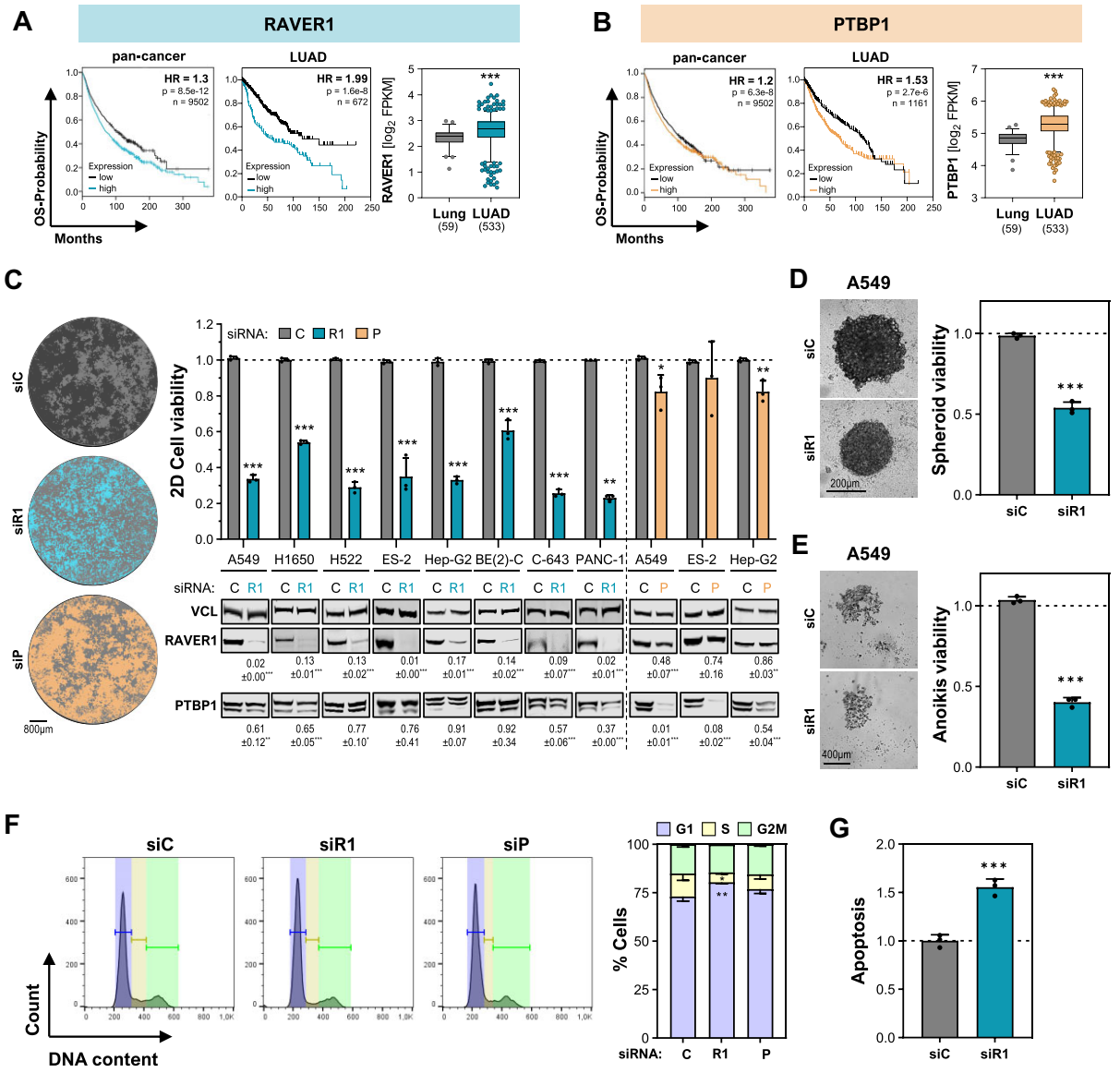

Figure 1. RAVER1 promotes tumor cell proliferation. (A, B) Kaplan–Meier and box plots of RAVER1 **(A)** and PTBP1 **(B)** overall survival probability and mRNA expression in 33 cancers (left panels) and LUAD (middle and right panels). HR, hazard ratio; *p*, log rank *p* value; *n*, number of analyzed samples. (**C–G**) Indicated cell line were transfected with RAVER1 (R1, turquoise), PTBP1 (P, apricot) or control (C, gray) siRNA pools for 24 h before cell splitting for the respective analyses. (C) Proliferation was determined by cell viability (upper panel). Representative images of A549 2D cell confluence are shown in the left panel. Representative Western blot analyses of RAVER1 and PTBP1 upon depletion are depicted in the bottom panel. Vinculin (VCL) serves as loading and normalization control. (D, E) Spheroid growth (D) and anoikis-resistance (E) of RAVER1-depleted A549 was determined by cell viability measurements. Representative images are shown in the left panels. (F) Cell cycle progression was determined upon propidium iodide staining of DNA via flow cytometry upon indicated knockdowns. (G) Apoptosis upon RAVER1 depletion in A549 was determined by caspase 3/7 activity. Measurements were normalized to the median of controls. Error bars indicate standard deviation and statistical significance was determined by Student's *t*-test: (*) $P < 0.05$, (**) $P < 0.01$, (***) $P < 0.001$.

RAVER1 deletion impairs tumor growth

To evaluate the oncogenic potential of RAVER1 in tumor growth, we established RAVER1-deleted A549 cell clones which notably showed barely affected PTBP1 expression (Figure 2A; Supplementary Figure S2A). Consistent with decreased proliferation observed upon transient RAVER1 depletion by two independent siRNA pools, RAVER1 knockout (KO) decreased cell growth in 2D, spheroid growth and most prominently anoikis resistance in two independent KO clones (Figure 2B–D). However, even though RAVER1-KO impaired proliferation, the re-expression of GFP-RAVER1 (~5-fold over endogenous RAVER1 levels in parental cells) failed to fully restore 2D proliferation (Supplementary Figure S2B). How RAVER1-KO influences tumor growth *in vivo* was investigated by subcutaneous (s.c.) xenograft models in nude mice (Figure 2E). To visualize tumor growth by non-invasive imaging, parental and RAVER1-KO A549 cells were stably transduced with iRFP (near infrared fluorescent protein) before s.c. injection (Figure 2F). The assessment of tumor growth by volume as well as endpoint tumor mass (after 25 days) indicated that RAVER1-KO led to significantly reduced tumor volume already two weeks after injection (Figure 2G–I). Tumors de-

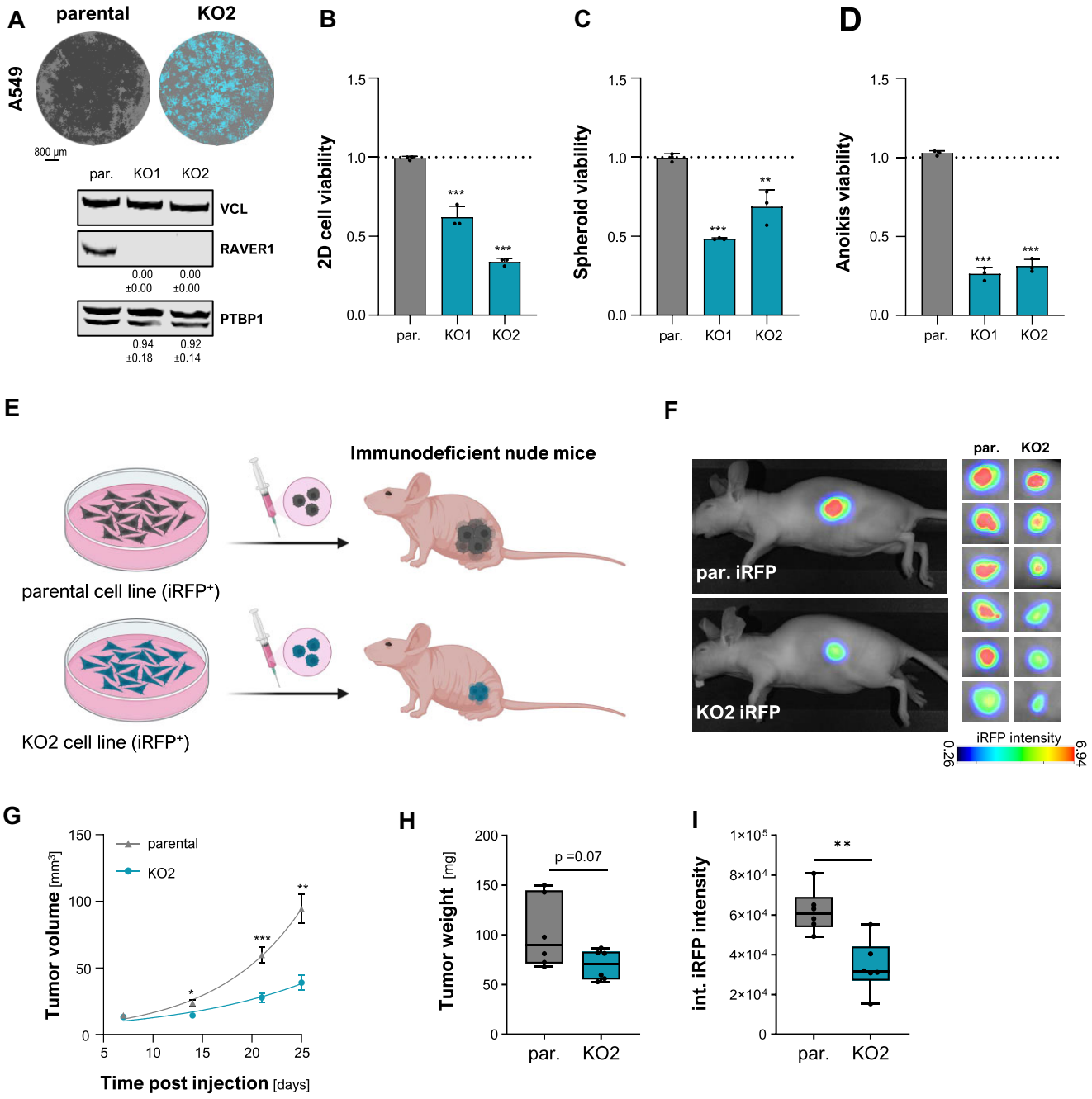

Figure 2. RAVER1 deletion impairs tumor growth. **(A)** Representative cell confluences (upper panel) and Western blot analysis (lower panel) of RAVER1 deletion by CRISPR/Cas9 in two independent A549 clones (KO, turquoise) versus parental cells (par., gray). (B–D) 2D cell proliferation **(B)**, spheroid growth **(C)**, and anoikis-resistance **(D)** were determined in RAVER1-KO (KO, turquoise) and parental cells (gray) by assessing cell viability. **(E–I)** Parental (gray) and RAVER1-deleted (KO2, turquoise) A549 cells expressing iRFP were injected (s.c.) into nude mice (6 per condition), as schematically shown in (E; BioRender, ZP25HKUDFM). The growth of xenografts was monitored by near-infrared imaging (IR). IR images of tumors, excised 25d post-injection, are shown in (F, intensity scale in bottom panel). Tumor volume over time (G), final tumor mass (H), and integrated final iRFP intensities of excised tumors (I) are shown. Error bars indicate standard deviation (B, C) or the standard error of mean (G). Statistical significance was determined by Student's *t*-test: (*) $P < 0.05$, (**) $P < 0.01$, (***) $P < 0.001$.

rived from parental A549 cells reached termination criteria at ~25 days post-injection, whereas volume remained ~2-fold smaller for RAVER1-KO derived tumors. Consistently, final tumor mass (H; $p = 0.07$) as well as integrated iRFP intensity (I; $p < 0.01$) was reduced by RAVER1-KO, providing strong evidence that RAVER1 serves pro-oncogenic roles in LUAD xenograft models by enhancing or maintaining elevated proliferation and tumor growth.

RAVER1 is dispensable for perinucleolar compartment (PNC) homeostasis

The original identification of RAVER1 revealed its association and co-localization with PTBPs in perinucleolar compartments (Supplementary Figure S3A) (17). Independent studies suggested elevated frequency of PNCs in progressed, metastatic malignancies (22,23). Accordingly, it was tempting to speculate that RAVER1's role in tumor cell proliferation is

associated with its potentially PTBP-dependent modulation of PNC homeostasis.

Whether RAVER1 is essential for the formation of and PTBP1-association with PNCs was analyzed in A549 cells depleted or deleted for RAVER1 (Figure 3A, B). Immunostaining of PTBP1 demonstrated that the recruitment of PTBP1 to PNCs was neither disturbed by RAVER1 depletion using two siRNA pools nor by RAVER1 deletion. Moreover, PNC frequency and size remained essentially unchanged by RAVER1 knockdown. In contrast to parental A549 cells (∼12% PNC-positive cells), however, we observed a substantial increase (KO1, ∼66% PNC-positive cells) or decrease (KO2, ∼1% PNC-positive cells) of PNC frequency by RAVER1-KO. Although PNC size was modestly decreased in KO1, these findings suggested that RAVER1 is largely dispensable for PNC homeostasis and that variations in PNC frequency observed in RAVER1-KO clones are due to clonal variability. In support of the latter, the investigation of PNC frequency in nine parental A549 single cell clones confirmed high variation of PNC frequency (Supplementary Figure S3B).

To address the role of RAVER1's N-terminal RRMs and C-terminal intrinsically disordered region (IDR) in PTBP1-association and PNC homeostasis, we established RAVER1-KO cell clones with stable re-expression of RAVER1 mutant proteins (Figure 3C). Affinity purification of SBP/FLAG-tagged RAVER1 proteins confirmed that the IDR and prior reported peptide motifs are essential for PTBP1-binding (Figure 3D). The role of RAVER1 domains in PNC recruitment and homeostasis was investigated by immunostaining of PTBP1 in RAVER1-KO cells expressing GFP or GFP-tagged RAVER1 mutant proteins (Figure 3E, Supplementary Figure S3C). In support of prior findings (17), GFP-tagged full-length RAVER1 showed stringent colocalization with PTBP1 in PNCs. In contrast to the ΔIDR mutant, the ΔRRM protein strongly associated with PNCs, confirming a pivotal role of the IDR in RAVER1-PNC association. However, the ΔRRM mutant protein also formed multiple GFP-positive aggregates throughout the nucleoplasm, suggesting a role of the N-terminal RRMs in preventing deregulated aggregation via the IDR outside of PNCs. Intriguingly, the PRI-mutant (cf. Figure 3C), which failed to associate with PTBP1, was evenly distributed throughout the nucleoplasm, suggesting that PTBP1-association is essential for the PNC-recruitment of RAVER1 (Figure 3E). The quantitative assessment of PNC frequency, size and PTBP1-association further implied that the full-length protein and IDR (ΔRRM) reduced the frequency of PNCs positive cells, whereas the RRMs (ΔIDR) enhanced the overall PNC size for unknown reasons. The PNC localization of PTBP1 remained essentially unchanged by the expression of RAVER1 variants. Collectively, these findings suggested that the IDR and PTBP1-association are essential for the localization of RAVER1 to PNCs. In contrast, the RRMs rather prevent unspecific aggregation of the protein in the nucleoplasm. Moreover, our findings reveal that PNCs are unlikely associated with RAVER1's oncogenic potential in tumor cells since both KO clones showed disturbed tumor cell growth but strikingly distinct PNC frequency.

RAVER1 depletion impairs proliferation pathways and promotes lethal EMT

Gene set enrichment analyses (GSEA) derived by RNAseq data in RAVER1-depleted A549 cells confirmed severe downregulation of pro-proliferative gene expression upon knockdown (Figure 4A; Supplementary Table TS6 and TS7). Essentially all pro-proliferative cancer hallmark gene sets (MsigDB-HM), most prominently E2F_target_genes (HM-E2F), were significantly decreased by RAVER1 knockdown, supporting the prior identified disturbance of G1/S transition and cell cycle progression (cf. Figure 1). Surprisingly, however, GSEA suggested induction of epithelial-mesenchymal-transition (EMT; HM_EMT) presumably due to elevated TGFB-signaling (HM_TGFβ) upon RAVER1 as well as PTBP1 knockdown (Figure 4A, B). Surprisingly, however, only the depletion of RAVER1 led to a robust and broad downregulation of conserved epithelial markers including E-cadherin (CDH1), upregulation of mesenchymal factors including N-cadherin (CDH2) and the EMT-driver SNAI2, as well as the enhancement of TGFBRs and TGFBI (Figure 4C; Supplementary Table TS6). This EMT-like shift in gene expression remained less stringent and comprehensive for PTBP1 knockdown. To address this in further detail, we investigated cell-cell contact homeostasis by staining of adherens junction (AJ) proteins and the actin cytoskeleton upon RAVER1 and PTBP1 depletion (Figure 4D; Supplementary Figure S4A). Consistent with partial EMT upon PTBP1 knockdown, cell-cell contacts remained pronounced with only moderate CDH2 localization to AJ sites and only slight re-organization of the microfilament system. In contrast, AJs were strongly enriched for CDH2, further reduced in number as well as density, and stress fibers appeared more mesenchymal-like in cells depleted for RAVER1 using two distinct siRNA pools. Depletion studies further indicated that neither PTBP1 nor RAVER1 knockdown led to a significant loss of CTNNB1 from AJs. EMT-like changes in cell morphology were also observed in both RAVER1 KO clones, supporting an EMT-inhibitory role of RAVER1 (Supplementary Figure S4D). In agreement, RAVER1 knockdown and deletion significantly enhanced the collective cell migration of A549 cells in wound closure analyses (Supplementary Figure S5A, B).

The concomitant reduction of proliferation and enhancement of apoptosis, EMT, as well as TGFB signaling by RAVER1 downregulation suggested the protein to limit lethal, TGFB-induced EMT (38). GSEA analyses in the MsigDB-C2 collection revealed a variety of TGFB-associated gene panels, which showed an overall similar enrichment (Pearson correlation: $R = 0.6043$, $P < 0.001$) for both, RAVER1 as well as PTBP1 depletion (Figure 4G; Supplementary Table TS7). However, two gene sets, both comprising changes in gene expression reported as lethal EMT or TGFB-induced apoptosis, stood out due to enrichment by RAVER1 depletion, whereas this was not seen for PTBP1 knockdown. Consistent with the induction of lethal EMT (38), RAVER1 depletion and deletion but not PTBP1 knockdown induced a strong enhancement of TGFB-driven facilitators of apoptosis, BIM (BCL2L11) as well as BMF and their drivers SMAD4 as well as SOX4 (Figure 4H, I; Supplementary Figure S5C, D). In addition, elevated SMAD4 expression in response to RAVER1 downregulation led to repression of KLF5 (Figure 4H, I), a prior reported hallmark of lethal EMT in PDAC (pancreatic ductal adenocarcinoma) models (39). Notably, elevated SMAD4 expression was restored by the re-expression of RAVER1 in KO cells (Supplementary Figure S5D), providing strong evidence for a key role of RAVER1 in limiting TGFB-driven, lethal EMT. This was analyzed in further detail by exposing

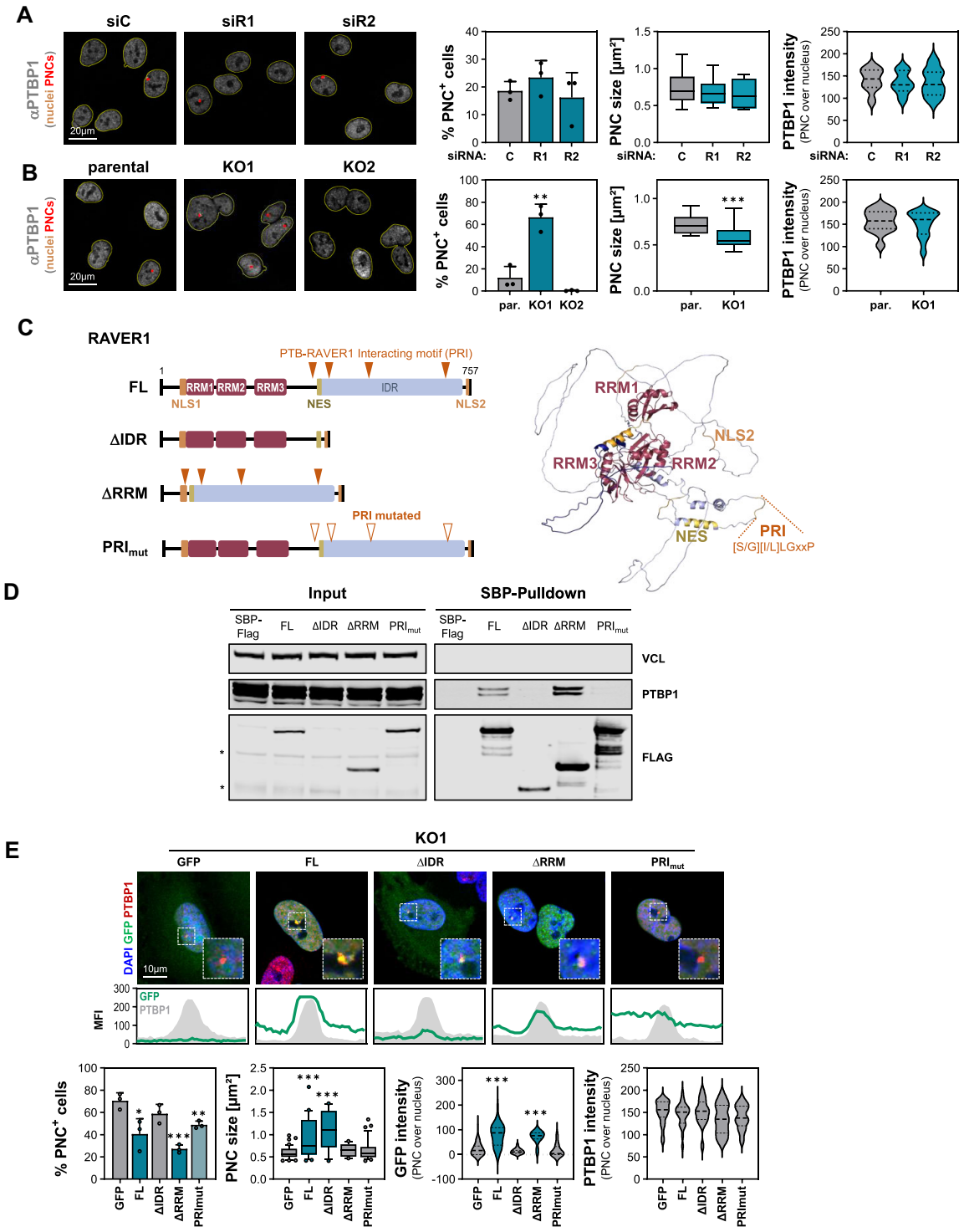

Figure 3. RAVER1 is dispensable for PNC homeostasis. **(A, B)** Immunostaining of PTBP1 upon control **(C)** and RAVER1-depletion (72h) using two distinct siRNA pools (A: R1, R2) and RAVER1-knockout (B: KO1, KO2) in parental A549 cells (B). Nuclei (yellow mask) and PNC (red mask) segmentation was performed using MiToBo NuclearParticleDetector (Fiji) to determine the percentage of PNC-positive cells (bar diagram), the PNC size distribution (box plot diagram), and PTBP1 mean fluorescence intensity (violin plots; normalized to mean fluorescence intensities (MFI) of nuclei). (C) Schematic of analyzed SBP/FLAG-tagged RAVER1 proteins with indicated motifs (left panel). Alphafold structure prediction of RAVER1 (E9PAU2, right panel) with N-terminal RRM domains, an extended intrinsically disordered C-terminal region, and sequence motifs. RRM, RNA-Recognition Motif; NLS, Nuclear Localization Signal; NES, Nuclear Export Signal; IDR, intrinsically disordered region; PRI, PTB-RAVER interacting motif. **(D)** Representative Western blot analysis of affinity purification of RAVER1 proteins indicated in (C) and re-expressed in KO1. (*) non-specific background. **(E)** Representative images of PTBP1-immunostaining (red), GFP-tagged RAVER1 proteins (green; re-expressed in KO1 cells), and nuclei (DAPI, blue) are shown in the upper panel. Dashed boxes depict enlarged region shown in the lower right corner. MFI profiles of RAVER1 (green) and PTBP1 (gray) are shown as the average of 10 PNCs in the middle panel. Quantifications of indicated parameters (lower panel) were performed as described in (A, B). Error bars indicate standard deviation of three independent analyses with a total of at least 50 cells analyzed per condition. Statistical significance was determined by Student's t-test: (*) $P < 0.05$, (**) $P < 0.01$, (***) $P < 0.001$.

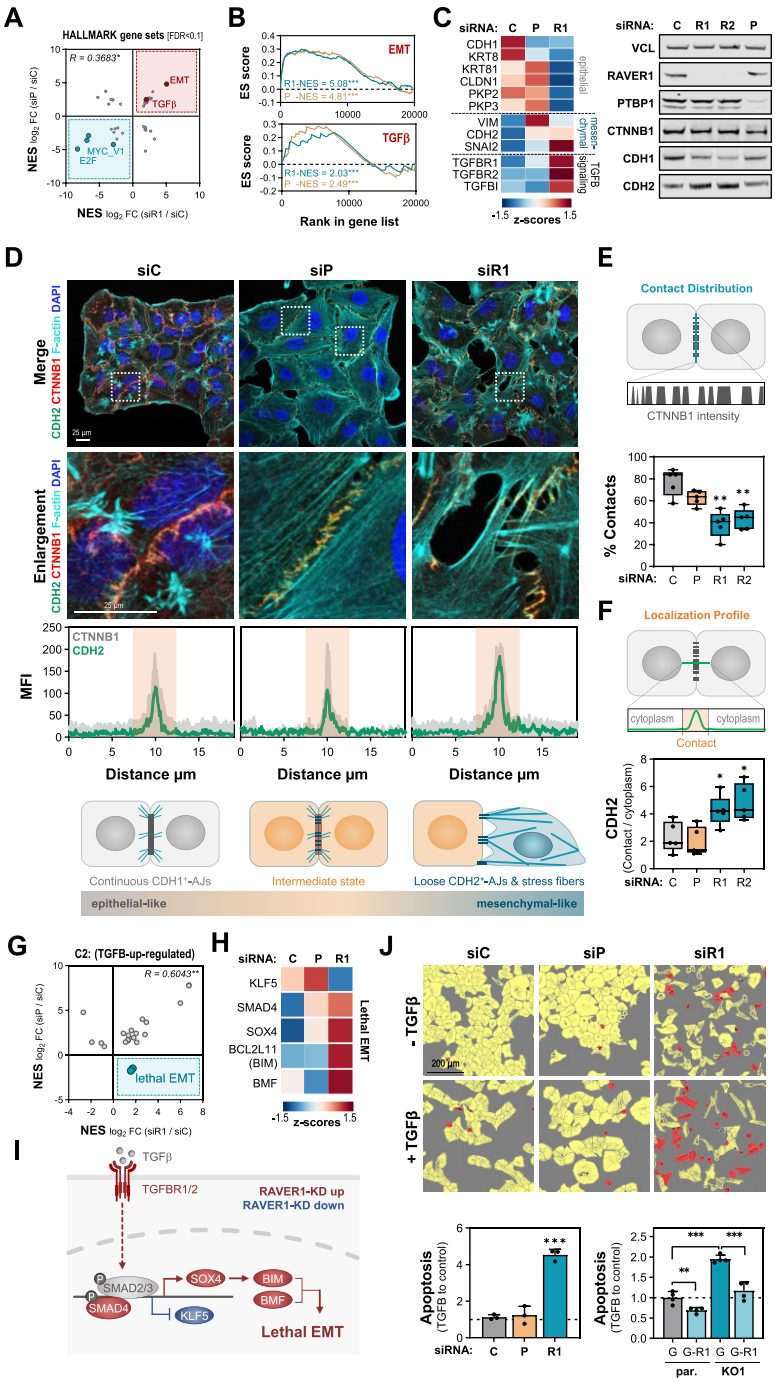

Figure 4. RAVER1 depletion impairs proliferation and promotes lethal EMT. (A, B) XY-presentation of normalized enrichment scores (NES) for Hallmark (HM) gene sets **(A)** and enrichment plots **(B)** of indicated gene sets as determined by GSEA upon RAVER1 (turquoise) and PTBP1 depletion (apricot) in A549 cells based on RNAseq data. ES, enrichment score. **(C)** Heat map of gene expression z-scores derived by RNAseq (left panel) and representative Western blot for indicated proteins upon depicted knockdowns (right panel). **(D)** Representative, merged images and enlargements of boxed regions (top panel) depicting CDH2 (green), CTNNB1 (red) immunostaining, F-actin (turquoise), and nuclei labeling (DAPI, blue) upon indicated depletions in A549 cells. MFI profiles (average of 10 cells) indicate CDH2 (green) and CTNNB1 (gray) at the site of cell-cell contacts (apricot) vs. the cytoplasm (middle panel). A schematic depicting altered adherens junction (AJ) morphology and EMT progression upon PTBP1 and RAVER1 knockdown is shown in the lower panel. (E, F) The percentage of cell-cell contacts as determined by CTNNB1 intensity at the membrane **(E)** and CDH2 contact-to-cytoplasm ratios **(F)**, determined according to schematics (upper panels), are shown by box plots summarizing five independent analyses and a total of at least 50 cells evaluated per condition. **(G)** XY-presentation of NES scores for TGFB-associated gene sets derived by GSEA in the C2 collection as described in (A). **(H)** Gene expression of lethal EMT markers as described in (C). **(I)** Scheme of TGFB-induced lethal EMT upon RAVER1 downregulation, according to (38,39). TGFB promotes the abundance of SOX4 (red) and SMAD2/3/4-dependent (unchanged, gray) synthesis of pro-apoptotic BIM, BMF (red), as well as downregulation of KLF5 (blue). **(J)** Representative images (upper panel) of segmentation masks for living (yellow) and apoptotic (red) cells determined by the AI Cell Health visualize cell morphology, for indicated treatments and depletions. Apoptosis depicted by bar diagrams (lower panels) was determined by normalizing Caspase 3/7 activity to cell content, essentially as in Figure 1G. Values are shown relative to controls for indicated knockdowns (lower left panel), RAVER1 overexpression (G: GFP; G-R1: GFP-RAVER1), and RAVER1 re-expression in KO1 (lower right panel). Error bars indicate standard deviation. Statistical significance was determined by Student's *t*-test: (*) $P < 0.05$, (**) $P < 0.01$, (***) $P < 0.001$.

A549 cells with RAVER1 or PTBP1 downregulation to TGFB (Figure 4J; Supplementary Figure S5E). Consistent with severe and selective (not observed for PTBP1 knockdown) upregulation of TGFBRs and SMAD4 by perturbed RAVER1 expression, TGFB-induced apoptosis was only observed in RAVER1 depleted and deleted A549 cells. Strikingly, the overexpression of RAVER1 reduced TGFB-induced apoptosis in parental cells and its re-expression essentially abolished TGFB-induced cell death in RAVER1-KO cells. In conclusion, this suggested that both, RAVER1 as well as PTBP1 influence TGFB signaling, but only RAVER1 is a strong inhibitor of TGFB-induced apoptosis and thus lethal EMT.

RAVER1 modulates miR/RISC activity in gene silencing

Aiming to unravel how RAVER1 and PTBP1 influence TGFB signaling, although to substantially distinct extent, we analyzed gene set enrichment in the MsigDB-C3 collection, containing gene panels with shared transcription factor targeting (TFT) as well as microRNA (miR, miRNA) targeting motifs. Strikingly, for miRNAs expressed in A549 cells (cpm > 10), RAVER1 as well as PTBP1 knockdown increased essentially all target gene panels (Figure 5A; Supplementary Table TS7). In contrast TFT gene panels showed a rather balanced distribution but overall downregulation. Inspection of the top five most depleted and enriched gene panels, however, emphasized substantial differences for RAVER1 versus PTBP1 knockdown (Figure 5B). In contrast to PTBP1, the downregulation of RAVER1 depleted various E2F-target gene sets, supporting a pronounced regulatory role in cell cycle progression by modulating G1/S transition and/or apoptosis (cf. Figure 1). Among enriched gene sets, PTBP1 as well as RAVER1 knockdown elevated miR-target gene panels. This supported previous findings suggesting PTBP1 to modulate miR/RISC-guided mRNA turnover (40). However, only RAVER1 knockdown concisely increased targets of (Figure 5B, C): the rather tumor-suppressive let-7 miRNA family (27), the oncomiR-21 with the exception of PDCD4 (24), and the EMT-suppressive miR-200 family (41,42). Notably, the miR-200 family is central for TGFB-induced cancerous EMT and maintaining epithelial integrity (41,42). This suggested that RAVER1's role in modulating TGFB-signaling involves regulation of miR/RISC activity leading to the upregulation of TGFBRs, SNAI2 and SMAD4 upon RAVER1 downregulation (Figure 5C). Along these lines, we hypothesized that deregulated expression of RAVER1 either disturbed miR biogenesis, turnover, or deregulated the activity of the miR/RISC machinery in a potentially mRNA-dependent manner. Northern blotting of total RNA isolated from RAVER1 and PTBP1 knockdown cells as well as RAVER1-KO clones showed that the abundance of miR-200b-3p, let7a-5p as well as miR-21–5p, the most frequent microRNA in carcinomas (24), remained essentially unchanged (Figure 5D). Thus, it appeared unlikely that the extensive upregulation of miR-target transcripts upon RAVER1 downregulation resulted from broadly decreased miRNA abundance. How disturbing RAVER1 and PTBP1 expression affects miR/RISC activity was tested by minimal luciferase reporters harboring one perfectly complementary miR-21-5p, let-7a-5p or miR-200c-3p targeting site in their 3′UTR (Figure 5E). RAVER1 but not PTBP1 knockdown significantly increased the activity of all these reporters. Strikingly, reporter activity was concisely elevated also by RAVER1 KO and restored by the re-expression of RAVER1. Collectively, these findings indicated that RAVER1 guides proper miR/RISC activity, which when disturbed leads to severely deregulated gene expression including the upregulation of TGFB signaling factors.

RAVER1 modulates alternative splicing in synergy with and independent of PTBP1

The reported role of RAVER1 in PTBP1-dependent alternative splicing (AS) suggested that RAVER1 influences miR/RISC activity at the level of AS, potentially in a partially PTBP1-independent manner. Therefore, shifts in splicing patterns were investigated by RNAseq in A549 cells upon RAVER1 as well as PTBP1 knockdown and data evaluation via rMATS (31).

Consistent with shRNA-directed PTBP1 knockdown in liver cancer-derived Hep-G2 cells (43), transient PTBP1 depletion by siRNAs in A549 cells predominantly impaired exon skipping and inclusion (Figure 6A; Supplementary Table TS8). This was also observed for RAVER1 knockdown, providing the first comprehensive evidence that RAVER1 mainly functions in the modulation of AS. The investigation of significant AS events (FDR < 0.05, |ΔPSI| > 0.05) in protein-coding genes revealed that both, RAVER1 as well as PTBP1 knockdown, promoted skipping as well as inclusion events in a nearly balanced manner and essentially indistinguishable exon width distribution (Figure 6B, C; Supplementary Figure S6A, B).

The comparison of 6472 significant (FDR 0.05, |ΔPSI| > 0.05) AS events in protein coding genes observed by RAVER1 and PTBP1 depletion unraveled an unexpectedly small overlap of 1204 (18.6%) AS events (Figure 6D). However, due to upregulation of PTBP2 by PTBP1 knockdown (cf. Supplementary Figure S1C), we cannot exclude partial recovery of PTBP1-dependent splicing by PTBP2. Irrespectively, shared splicing events (RAVER1 and PTBP1) showed strongly coherent regulation, evidenced by positive Pearson correlation ($R = 0.72$, $P < 0.0001$) and more skipping (656, 54.5%) than inclusion (412, 34.2%), supporting previously reported co-regulation in AS by both proteins. GSEA analyses based on gene ranking by PSI values failed to reveal any enrichment of gene panels among coherently, shared AS events (data not shown). GO term analyses of PTBP1-only, RAVER1-only or shared target genes suggested a moderate enrichment of genes encoding proteins implicated in cytoskeletal protein binding among shared and PTBP1-only events. This was slightly distinct for RAVER1 which preferentially modulated factors involved in catalytic_acting_on_DNA activity (Supplementary Figure S6D and Supplementary Table TS9). Thus, despite overlapping regulatory roles, these findings implied that RAVER1 and PTBP1 also serve independent roles in the control of AS.

Hexamer motif analyses in exons differentially regulated by RAVER1 and PTBP1 indicated partially distinct motif enrichment in skipping versus inclusion events (Figure 6E; Supplementary Figure S6C and Supplementary Table TS10). The range of enrichment was similar to hexamer distribution observed for SRFS4/6-dependent, hypoxia-associated AS in cancer cells (44). Strikingly, CU-enriched motifs were enhanced within AS exons deregulated by RAVER1 as well as PTBP1 knockdown. Likewise, a similar, yet in part distinct enrichment was observed for RBP-binding motifs within AS exons, especially motifs reported for other splicing regulators

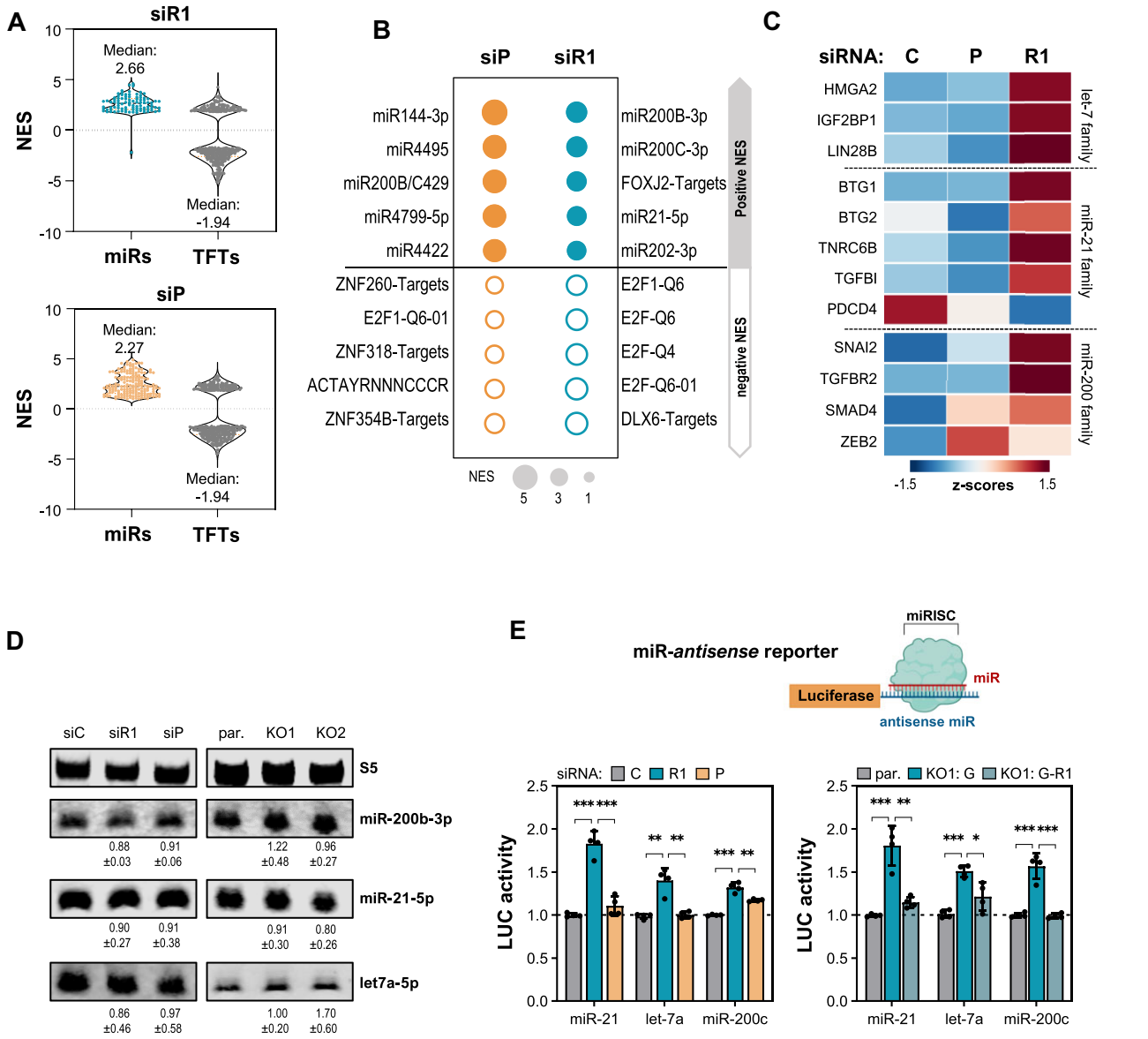

Figure 5. RAVER1 modulates the miR/RISC-guided control of gene expression. **(A)** Violin plots of normalized enrichment scores (NES; FDR < 0.05) determined by GSEA in the C3-MIR (miRNAs; colored) and C3-TFT (transcription factor targets, gray) collections upon indicated depletion in A549 cells. **(B)** NES values of the top five C3-all gene sets (A) are shown by bubble charts. **(C)** Heat map showing median-normalized z-scores for altered expression of indicated miR-target mRNAs upon depicted knockdowns. **(D)** Northern blot analyses of indicated microRNAs upon depicted knockdowns (left panel) and RAVER1 deletion (right panel) in A549 cells. **(E)** Schematic of miR-anti-sense luciferase reporters (upper panel; BioRender, KV25HKUK72). Normalized activity of indicated reporters is shown by bar diagrams for RAVER1 and PTBP1 depletion (lower left panel), RAVER1 deletion and RAVER1 re-expression in A549 cells (lower right panel). Error bars show standard deviation and statistical significance was determined by Student's *t*-test: (*) $P < 0.05$, (**) $P < 0.01$, (***) $P < 0.001$.

like SRSFs (Supplementary Table TS10). These findings suggested that RAVER1, like proposed for its association with PTBP1 (18), modulates splicing by complexing with a variety of other splicing regulators. According to protein association reported by BioGRID, RAVER1 was proposed to associate with various RBPs, including SRSFs (Supplementary Table TS11). This was analyzed in further detail in RAVER1-KO A549 cells, re-expressing SBP/FLAG-tagged RAVER1 or SBP/FLAG, serving as control. The investigation of proteins co-purified with RAVER1 by LC–MS/MS confirmed purification of RAVER1 and association with PTBP1 (Figure 6F; Supplementary Figure S6E and Supplementary Table TS12). In addition, RAVER1 bound SRSFs, for instance SRSF2 which showed enriched motifs in RAVER1-controlled exons (Supplementary Table TS10 and TS12), and other splicing regulators like PCBP1. In agreement, GSEA in the C2-reactome collection indicated significant enrichment of mRNA processing and elevation of splicing regulators among RAVER1-associated proteins (Figure 6F; Supplementary Table TS12).

RAVER1 is a master regulator of alternative splicing within the miR/RISC pathway

The analysis of gene enrichment among deregulated splicing events upon RAVER1 and PTBP1 depletion did not highlight factors implicated in the control of miR/RISC activity. Therefore, we investigated a list of 30 factors with validated roles in miR biogenesis, miR/RISC activity, and miR

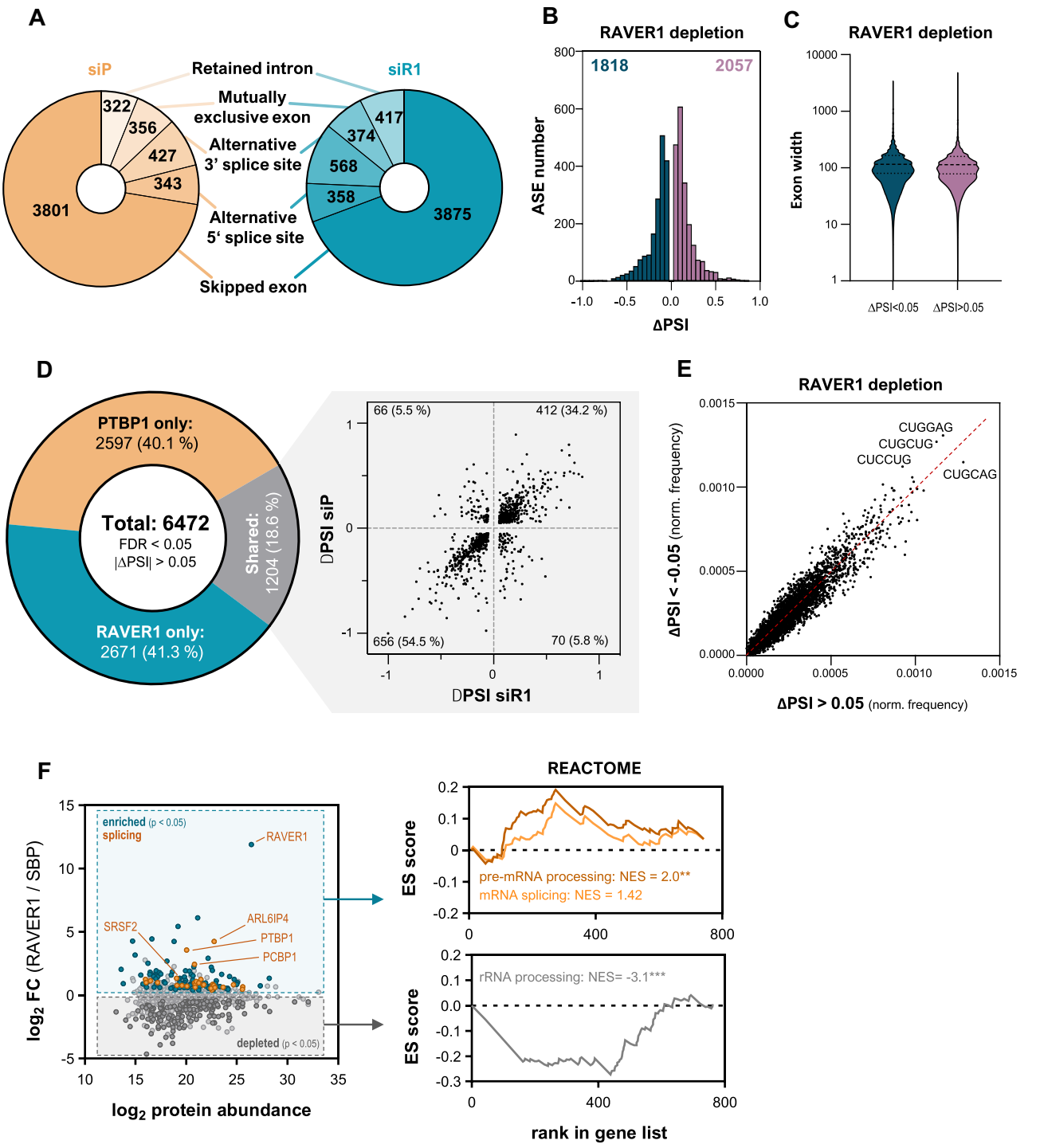

Figure 6. RAVER1 modulates alternative splicing. (A–C) Pie char depiction **(A)** of significant rMATS-reported splicing events upon RAVER1 (turquoise) and PTBP1 (apricot) depletion in A549 cells. Events were filtered for protein coding transcripts, FDR < 0.05, and |ΔPSI| > 0.05. ΔPSI value **(B)** and exon width **(C)** distributions of significant alternative splicing (AS) events upon RAVER1 knockdown are shown by frequency plots and violin plots, respectively. **(D)** Pie chart depicting the relative amount of PTBP1 only (apricot), RAVER1 only (turquoise) and shared (RAVER1 and PTBP1) AS events. An XY-correlation plot for shared AS events is shown in the right panel with absolute and relative event numbers indicated in each quadrant. **(E)** XY-presentation of hexamer frequency in alternatively spliced exons for indicated ΔPSI values upon RAVER1 knockdown in A549 cells. **(F)** LC–MS/MS analyses of proteins co-purified with SBP/FLAG-RAVER1 from RAVER1-KO1 cells re-expressing SBP/FLAG (control) or SBP/FLAG-RAVER1. The log2 enrichment of proteins with RAVER1 is shown by XY-presentation over log2 protein expression (left panel). Significantly ($P < 0.05$) enriched proteins are indicated by color. ES score plots shown in the right panels were derived by GSEA for indicated C2/Reactome gene sets using fold enrichment of proteins for ranking.

decay derived from recent overview articles (45,46). Strikingly, hypergeometric testing indicated a ∼3.3-fold enrichment (21/30 genes, $P = 1.2e^{-08}$) of disturbed AS within the miR/RISC pathway upon RAVER1 depletion (Figure 7A; Supplementary Table TS13). This deregulation was less pronounced for PTBP1 knockdown (∼1.9-fold enrichment, 12/30 genes, $P = 0.01$; Supplementary Table TS13). The evaluation of selected AS events by semi-quantitative RT-PCR largely confirmed disturbed isoform synthesis, as determined by rMATS, with a validation rate of ∼90% (Figure 7B, C; Supplementary Figure S7). Moreover, for selected AS events, deregulated splicing due to disturbed RAVER1 was confirmed by depletion using independent siRNA pools, RAVER1-KO as well as restored splicing upon re-expression of RAVER1 in KO cells (Figure 7C; Supplementary Figure S8). Notably, most splicing events within miR/RISC pathway genes were mainly (e.g. TNRC6B) or exclusively (e.g. TNRC6C) controlled by RAVER1, which may contribute to distinct deregulation of miR/RISC activity by RAVER1 versus PTBP1 downregulation. In addition, to changing AS in the miR/RISC pathway, RAVER1 knockdown also altered the overall abundance of some key effectors of miR/RISC activity (Figure 7A; Supplementary Table TS13). This was most prominently observed by significant upregulation of all three TNRC6 proteins, which are essential for miR-induced mRNA decay due to linking AGO2 and the 3′-decay machinery of mRNAs (45,46). Essential for this bridging function of TNRC6 proteins is their association with AGO2 via GW-enriched, intrinsically disordered regions (47), present within all three TNRC6 paralogues (Figure 7D). The downregulation of RAVER1 modulated alternative splicing of AGO2-binding, GW-rich motifs (GW-II or GW-III, also termed AGO hook domain) in all three TNRC6 proteins. This deregulation of AS resulted in TNRC6 proteins with a higher relative GW content due to insertion of additional GW motifs (TNRC6A and TNRC6B) or skipping of GW-devoid regions (TNRC6C) in AGO-binding GW-rich regions. If alternative composition of the AGO hook domain indeed affects AGO2 association was analyzed for exon 6 of TNRC6B. IP studies from co-transfected HEK293T cells showed that deletion of this exon significantly reduced GFP-AGO2 association of truncated TNRC6B proteins, comprising GW-II (Figure 7E). In summary, these studies suggested that RAVER1 modulates miR/RISC activity by guiding alternative splicing and impacting on the abundance of various miR/RISC pathway genes, specifically factors involved in gene silencing by miR/RISC complexes.

Discussion

The RAVER1 protein has been considered one of several co-factors synergizing with the key splicing regulatory PTBP protein family (16,17), which has been implicated in cancer progression (10). In this study, we provide the first evidence that RAVER1 is a pro-oncogenic modulator of alternative splicing (AS) in cancer cells, which controls splicing in concert with as well as independent of PTBP1. Unexpectedly, RAVER1 depletion/deletion impaired tumor cell fitness in a more robust and conserved manner than PTBP1 knockdown. In s.c. LUAD (A549) xenograft mouse models, the loss of RAVER1 even reduced tumor growth, indicating that RAVER1 serves a rather pro-oncogenic role in lung and presumably other cancers. PTBPs and RAVER1 associate and co-localize in perinucleolar compartments (PNCs, (17)), which were proposed to be enhanced in progressed malignancies (22,23). Thus, it was tempting to speculate that RAVER1 modulates tumor cell fate in a PNC-dependent manner. However, in lung cancer cells, PNC number and integrity was not strictly associated with RAVER1 abundance but rather varied due to clonal variability. Depletion, deletion, and re-expression studies clearly indicate that RAVER1 associates with PNCs via its intrinsically disordered region and in a PTBP1-binding dependent manner but is not essential for PNC assembly. Thus, it appears unlikely that RAVER1 promotes tumor growth and survival in a strongly PNC-associated manner.

The characterization of deregulated gene expression upon RAVER1 downregulation confirmed the observed defects in proliferation and apoptosis. Unexpectedly, however, RAVER1 downregulation elevated TGFB signaling, epithelial-mesenchymal-transition (EMT) and strongly enhanced lethal EMT upon exposure to TGFB. The latter was proposed to promote tumor cell death in a SMAD2,3,4/KLF5-repressive as well as SMAD2,3,4/SOX4-simulated manner leading to elevated apoptosis due to BIM/BMF upregulation (38,39). Consistently, RAVER1 but not PTBP1 depletion elevated SMAD4, SOX4, BIM, and BMF, but decreased KLF5. Importantly, among these key regulators of lethal EMT, only BIM shows deregulated splicing upon RAVER1 depletion. This suggests that RAVER1 limits TGFB-induced apoptosis and EMT largely by restricting the abundance of key facilitators of TGFB signaling, most prominently TGFBR1/2 and SMAD4. The control of cancerous EMT and induction of lethal EMT essentially relies on the upregulation of central TGFB signaling factors, including TGFBR1/2, and enhanced expression of the EMT-driving transcription factor families SNAIs, TWISTs and ZEBs (48). Pivotal inhibitors of this process are microRNAs, in particular the miR-200 family, which impairs the synthesis of TGFB signaling components, including TGFBRs, as well as EMT-driving transcription factors (41,42). Our studies demonstrate that RAVER1 is a broad modulator of miR/RISC activity, but barely affects miR biogenesis. This regulatory role is associated with a substantial number of miR/RISC pathway genes subjected to control of AS by RAVER1. The multitude of splicing events modulated by RAVER1 within the miR/RISC pathway, affecting 21 of 30 major pathway genes, in conjunction with disturbed expression of some components, e.g. TNRC6 proteins, prohibits the identification of prime events via which RAVER1 modulates miR/RISC activity. Moreover, the evaluation of RAVER1-modulated splicing events in TNRC6 proteins provide strong evidence for a RAVER1-dependent modulation of protein interactions guiding miR/RISC activity. This was evaluated here for TNRC6-AGO2 association relying on GW-enriched regions in TNRC6 proteins (45). The fine-tuning of these interactions by shifting the isoform composition and abundance of miR/RISC pathway factors likely influences the activity and cooperativity of miR/RISC complexes, in a potentially partially mRNA-dependent but generally broad manner (49). Obviously, the combination of increased GW-content and abundance of TNRC6 proteins does not induce elevated miR/RISC activity. This suggests that isoform composition and abundance of miR/RISC factors need to be balanced to ensure proper miR/RISC activity. In addition, RAVER1 likely influences the nuclear as well as cytoplasmic functions of the CCR4/NOT complex

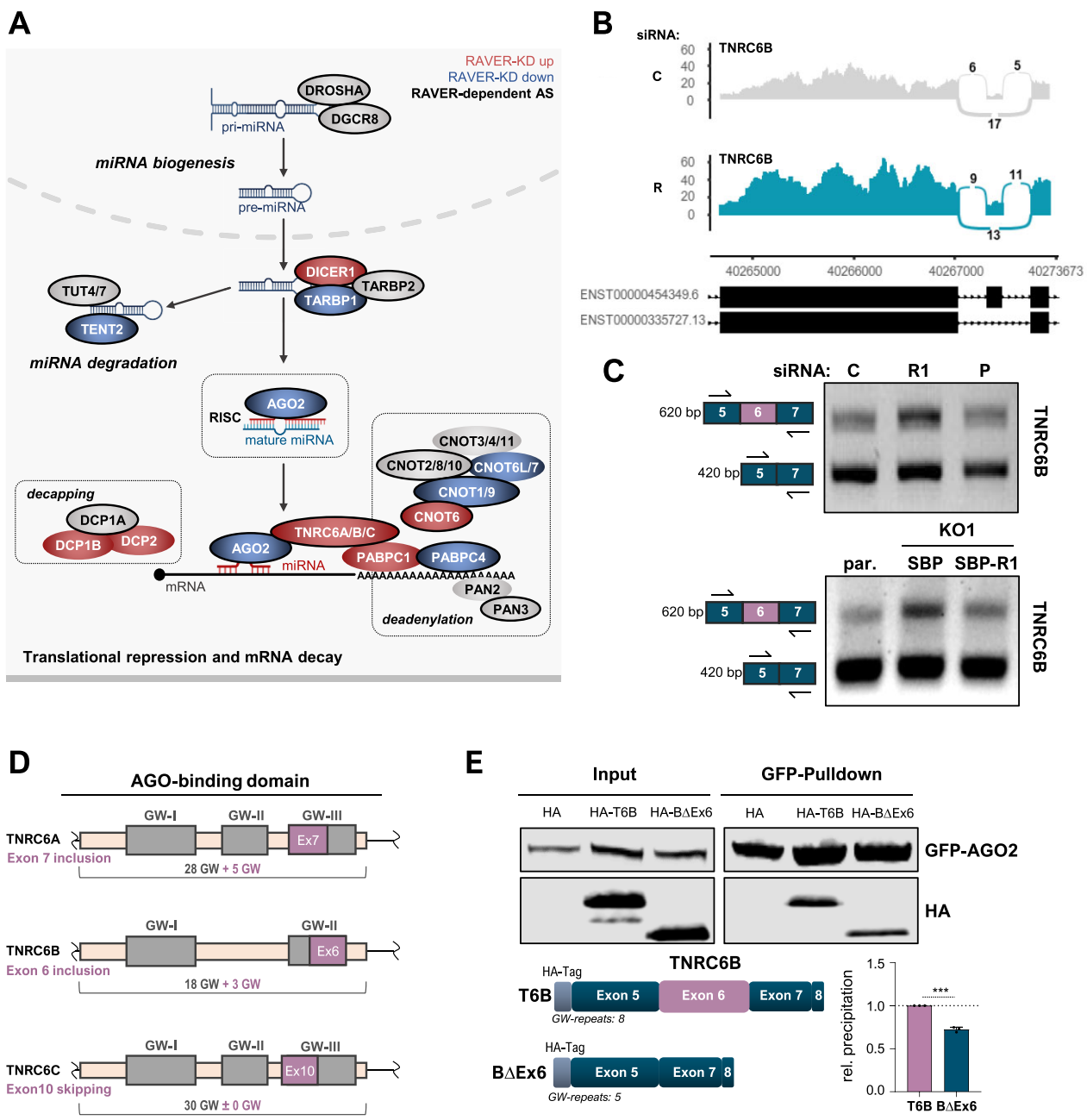

Figure 7. RAVER1 is a key regulator of alternative splicing in the miR/RISC pathway. **(A)** Scheme of essential facilitators of miR-processing and miR/RISC activity in gene silencing, as derived from (45,46). The color code indicates significantly enhanced (red), decreased (blue), non-significantly altered (gray) mRNA expression upon RAVER1 knockdown. Black shape outlines indicate at least one significant AS event for the respective genes in response to RAVER1 depletion in A549 cells. For details, please refer to Supplementary Table S13. **(B)** Sashimi plot of TNRC6B splicing in RAVER1-depleted A549 cells, as determined by rMATS. **(C)** Semi-quantitative RT-PCR analysis of alternative splicing of exon 6 in TNRC6B (scheme in left panel) in response to indicated knockdowns (upper panel) and the re-expression of SBP/FLAG-tagged RAVER1 in the KO1 clone. **(D)** Scheme of GW-rich clusters in the AGO-binding regions of TNRC6 proteins with alternatively spliced exons (light purple) and altered GW content upon alternative transcript processing. **(E)** Representative Western blot (upper panel) showing copurification of schematically depicted (left lower panel) TNRC6B protein fragments with immunopurified GFP-AGO2. TNRC6B proteins include (T6B) or lack (BΔEx6) the GW-rich exon 6, which is alternatively spliced upon RAVER1 knockdown. Quantification of TNRC6B protein copurification determined in three independent studies by normalization to purified GFP-AGO2 amounts is shown in a bar diagram (lower right panel). Error bars show standard deviation and statistical significance was determined by Student's *t*-test: (***) $P < 0.001$.

(50). RAVER1 associates with CCR4/NOT components, especially the scaffolding factor CNOT1, and extensively modulates splicing of most CCR4/NOT factors. How this influences CCR4/NOT functions and if this also provides a rationale for the potentially mRNA-specific modulation of miR-in/dependent deadenylation (51), requires further investigation. Furthermore, our studies cannot exclude that RAVER1-controlled alternative splicing within the TGFB signaling pathway itself, e.g. in TGFBRs, or other signaling pathways may contribute to the observed phenotypic consequence observed by RAVER1 downregulation. However, the strong upregulation of TGFBRs, TGFB signaling, lethal EMT and broadly disturbed miR/RISC activity observed by the downregulating RAVER1, provide strong evidence that RAVER1 is a potent guard of proper miR/RISC activity, which limits TGFB signaling to prevent TGFB-induced apoptosis.

In addition to providing the first mechanistic insights into how RAVER1 controls tumor cell fate, our studies also present the first transcriptome-wide investigation of the RAVER1-dependent control of splicing. So far, RAVER1 was considered to primarily serve as a co-factor of PTBP-dependent splicing (5,16,19). Our findings, confirm this synergy of PTBP1 and RAVER1 in controlling more than 1000 AS events in A549 cells. However, we also observe that RAVER1 regulates even more AS events (> 2500) largely independent of PTBP1. These findings may be biased, at least partially, by PTBP2 upregulation in PTBP1 depleted cells. However, the association of RAVER1 with other modulators of splicing, for instance SRSF proteins and PCBP1, supports the notion that RAVER1 modulates splicing not exclusively in concert with PTBPs. Whether co-regulation with PTBPs or other splicing factors involves direct association of RAVER1 with target transcripts remains to be determined. Attempts to evaluate RAVER1-RNA association by STAMP (Surveying Targets by APOBEC-Mediated Profiling, (52)) so far failed to reveal preferred binding substrates of RAVER1 (data not shown). This favors the view that RAVER1 mainly acts as a co-factor orchestrating the assembly of regulatory protein complexes guiding AS control, as already proposed for its synergistic regulation with PTBPs (18). The assembly of such multi-protein complexes on pre-mRNAs likely settles on RAVER1's extended IDR, which is essential for its association with PTBPs and the recruitment to PNCs. By acting in concert with such factors, RAVER1 likely modulates a multitude of AS events affecting tumor cell fate and the innate immune response (IIR). This was proposed due to RAVER1's association with MDA5 and roles in modulating SARS-CoV-2 infections in human and primate cell models (53,54). However, protein interactions, molecular mechanisms and key splicing substrates implicated in RAVER1's role in the IIR remain to be determined.

Data availability

RNA sequencing data are available in the Gene Expression Omnibus under accession code GSE232714. Proteomic data were uploaded to Pride under accession code PXD043342.

Supplementary data

Supplementary Data are available at NAR Online.

Acknowledgements

The authors thank the Core Facility Imaging (CFI) and core unit for NGS analyses of the Martin Luther University (MLU) for broad support with image and NGS data analysis.

Author contributions: A.W. and S.H. designed the experiments. A.W., N.B., S.M., A.R, M.L., J. U., KB.O., T.S., LM.P., C.M., T.F., C.I. and R.J. performed experimental studies. M.G., L.S., and S.H. supported data analysis and interpretation. M.K., T.G. and A.S. supported experimental design and data interpretation. S.H. conceived the experimental design and wrote the manuscript. Schemes were created with BioRender.com.

Funding

Stefan Hüttelmaier, Andrea Sinz and Marcel Köhn [DFG-RTG2467, 391498659]; Tony Gutschner [DFG, 440716364]; Nadine Bley and Stefan Hüttelmaier [DFG-FOR5433, 468534282]. Funding for open access charge: State funding.

Conflict of interest statement

None declared.

References

1. Marasco,L.E. and Kornblihtt,A.R. (2023) The physiology of alternative splicing. *Nat. Rev. Mol. Cell Biol.*, **24**, 242–254.
2. Bonnal,S.C., Lopez-Oreja,I. and Valcarcel,J. (2020) Roles and mechanisms of alternative splicing in cancer - implications for care. *Nat. Rev. Clin. Oncol.*, **17**, 457–474.
3. Zhang,Y., Qian,J., Gu,C. and Yang,Y. (2021) Alternative splicing and cancer: a systematic review. *Signal Transduct. Target Ther.*, **6**, 78.
4. Spellman,R., Rideau,A., Matlin,A., Gooding,C., Robinson,F., McGlincy,N., Grellscheid,S.N., Southby,J., Wollerton,M. and Smith,C.W. (2005) Regulation of alternative splicing by PTB and associated factors. *Biochem. Soc. Trans.*, **33**, 457–460.
5. Llorian,M., Schwartz,S., Clark,T.A., Hollander,D., Tan,L.Y., Spellman,R., Gordon,A., Schweitzer,A.C., de la Grange,P., Ast,G., *et al.* (2010) Position-dependent alternative splicing activity revealed by global profiling of alternative splicing events regulated by PTB. *Nat. Struct. Mol. Biol.*, **17**, 1114–1123.
6. Singh,R., Valcarcel,J. and Green,M.R. (1995) Distinct binding specificities and functions of higher eukaryotic polypyrimidine tract-binding proteins. *Science*, **268**, 1173–1176.
7. Oberstrass,F.C., Auweter,S.D., Erat,M., Hargous,Y., Henning,A., Wenter,P., Reymond,L., Amir-Ahmady,B., Pitsch,S., Black,D.L., *et al.* (2005) Structure of PTB bound to RNA: specific binding and implications for splicing regulation. *Science*, **309**, 2054–2057.
8. Black,D.L. (2003) Mechanisms of alternative pre-messenger RNA splicing. *Annu. Rev. Biochem.*, **72**, 291–336.
9. Ye,R., Hu,N., Cao,C., Su,R., Xu,S., Yang,C., Zhou,X. and Xue,Y. (2023) Capture RIC-seq reveals positional rules of PTBP1-associated RNA loops in splicing regulation. *Mol. Cell*, **83**, 1311–1327.
10. Zhu,W., Zhou,B.L., Rong,L.J., Ye,L., Xu,H.J., Zhou,Y., Yan,X.J., Liu,W.D., Zhu,B., Wang,L., *et al.* (2020) Roles of PTBP1 in alternative splicing, glycolysis, and oncogensis. *J. Zhejiang Univ. Sci. B*, **21**, 122–136.
11. Ni,T., Chu,Z., Tao,L., Zhao,Y., Zhu,M., Luo,Y., Sunagawa,M., Wang,H. and Liu,Y. (2023) PTBP1 drives c-myc-dependent gastric cancer progression and stemness. *Br. J. Cancer*, **128**, 1005–1018.
12. Chen,C., Shang,A., Gao,Y., Huang,J., Liu,G., Cho,W.C. and Li,D. (2022) PTBPs: an immunomodulatory-related prognostic biomarker in pan-cancer. *Front. Mol. Biosci.*, **9**, 968458.

13. Shinohara,H., Kumazaki,M., Minami,Y., Ito,Y., Sugito,N., Kuranaga,Y., Taniguchi,K., Yamada,N., Otsuki,Y., Naoe,T., *et al.* (2016) Perturbation of energy metabolism by fatty-acid derivative AIC-47 and imatinib in BCR-ABL-harboring leukemic cells. *Cancer Lett.*, **371**, 1–11.
14. Mereau,A., Anquetil,V., Lerivray,H., Viet,J., Schirmer,C., Audic,Y., Legagneux,V., Hardy,S. and Paillard,L. (2015) A posttranscriptional mechanism that controls Ptbp1 abundance in the *Xenopus epidermis*. *Mol. Cell. Biol.*, **35**, 758–768.
15. Wollerton,M.C., Gooding,C., Wagner,E.J., Garcia-Blanco,M.A. and Smith,C.W. (2004) Autoregulation of polypyrimidine tract binding protein by alternative splicing leading to nonsense-mediated decay. *Mol. Cell*, **13**, 91–100.
16. Gromak,N., Rideau,A., Southby,J., Scadden,A.D., Gooding,C., Huttelmaier,S., Singer,R.H. and Smith,C.W. (2003) The PTB interacting protein raver1 regulates alpha-tropomyosin alternative splicing. *EMBO J.*, **22**, 6356–6364.
17. Huttelmaier,S., Illenberger,S., Grosheva,I., Rudiger,M., Singer,R.H. and Jockusch,B.M. (2001) Raver1, a dual compartment protein, is a ligand for PTB/hnRNPI and microfilament attachment proteins. *J. Cell Biol.*, **155**, 775–786.
18. Rideau,A.P., Gooding,C., Simpson,P.J., Monie,T.P., Lorenz,M., Huttelmaier,S., Singer,R.H., Matthews,S., Curry,S. and Smith,C.W. (2006) A peptide motif in Raver1 mediates splicing repression by interaction with the PTB RRM2 domain. *Nat. Struct. Mol. Biol.*, **13**, 839–848.
19. Keppetipola,N.M., Yeom,K.H., Hernandez,A.L., Bui,T., Sharma,S. and Black,D.L. (2016) Multiple determinants of splicing repression activity in the polypyrimidine tract binding proteins, PTBP1 and PTBP2. *RNA*, **22**, 1172–1180.
20. Coelho,M.B., Ascher,D.B., Gooding,C., Lang,E., Maude,H., Turner,D., Llorian,M., Pires,D.E., Attig,J. and Smith,C.W. (2016) Functional interactions between polypyrimidine tract binding protein and PRI peptide ligand containing proteins. *Biochem. Soc. Trans.*, **44**, 1058–1065.
21. Norton,J.T. and Huang,S. (2013) The perinucleolar compartment: RNA metabolism and cancer. *Cancer Treat. Res.*, **158**, 139–152.
22. Kamath,R.V., Thor,A.D., Wang,C., Edgerton,S.M., Slusarczyk,A., Leary,D.J., Wang,J., Wiley,E.L., Jovanovic,B., Wu,Q., *et al.* (2005) Perinucleolar compartment prevalence has an independent prognostic value for breast cancer. *Cancer Res.*, **65**, 246–253.
23. Gonzalez,E., Ahmed,A.A., McCarthy,L., Chastain,K., Habeebu,S., Zapata-Tarres,M., Cardenas-Cardos,R., Velasco-Hidalgo,L., Corcuera-Delgado,C., Rodriguez-Jurado,R., *et al.* (2023) Perinucleolar compartment (PNC) prevalence as an independent prognostic factor in pediatric ewing sarcoma: a multi-institutional study. *Cancers (Basel)*, **15**, 2230.
24. Muller,S., Wedler,A., Breuer,J., Glass,M., Bley,N., Lederer,M., Haase,J., Misiak,C., Fuchs,T., Ottmann,A., *et al.* (2020) Synthetic circular miR-21 RNA decoys enhance tumor suppressor expression and impair tumor growth in mice. *NAR Cancer*, **2**, zcaa014.
25. Zinnall,U., Milek,M., Minia,I., Vieira-Vieira,C.H., Muller,S., Mastrobuoni,G., Hazapis,O.G., Del Giudice,S., Schwefel,D., Bley,N., *et al.* (2022) HDLBP binds ER-targeted mRNAs by multivalent interactions to promote protein synthesis of transmembrane and secreted proteins. *Nat. Commun.*, **13**, 2727.
26. Muller,S., Bley,N., Busch,B., Glass,M., Lederer,M., Misiak,C., Fuchs,T., Wedler,A., Haase,J., Bertoldo,J.B., *et al.* (2020) The oncofetal RNA-binding protein IGF2BP1 is a druggable, post-transcriptional super-enhancer of E2F-driven gene expression in cancer. *Nucleic Acids Res.*, **48**, 8576–8590.
27. Busch,B., Bley,N., Muller,S., Glass,M., Misiak,D., Lederer,M., Vetter,M., Strauss,H.G., Thomssen,C. and Huttelmaier,S. (2016) The oncogenic triangle of HMGA2, LIN28B and IGF2BP1 antagonizes tumor-suppressive actions of the let-7 family. *Nucleic Acids Res.*, **44**, 3845–3864.
28. Wisniewski,J.R., Zougman,A., Nagaraj,N. and Mann,M. (2009) Universal sample preparation method for proteome analysis. *Nat. Methods*, **6**, 359–362.
29. Bley,N., Schott,A., Muller,S., Misiak,D., Lederer,M., Fuchs,T., Assmann,C., Glass,M., Ihling,C., Sinz,A., *et al.* (2021) IGF2BP1 is a targetable SRC/MAPK-dependent driver of invasive growth in ovarian cancer. *RNA Biol.*, **18**, 391–403.
30. Bley,N., Lederer,M., Pfalz,B., Reinke,C., Fuchs,T., Glass,M., Moller,B. and Huttelmaier,S. (2015) Stress granules are dispensable for mRNA stabilization during cellular stress. *Nucleic Acids Res.*, **43**, e26.
31. Shen,S., Park,J.W., Lu,Z.X., Lin,L., Henry,M.D., Wu,Y.N., Zhou,Q. and Xing,Y. (2014) rMATS: robust and flexible detection of differential alternative splicing from replicate RNA-seq data. *Proc. Natl. Acad. Sci. U.S.A.*, **111**, E5593–E5601.
32. Frankish,A., Diekhans,M., Jungreis,I., Lagarde,J., Loveland,J.E., Mudge,J.M., Sisu,C., Wright,J.C., Armstrong,J., Barnes,I., *et al.* (2021) Gencode 2021. *Nucleic Acids Res.*, **49**, D916–D923.
33. Garrido-Martin,D., Palumbo,E., Guigo,R. and Breschi,A. (2018) ggsashimi: sashimi plot revised for browser- and annotation-independent splicing visualization. *PLoS Comput. Biol.*, **14**, e1006360.
34. Quinlan,A.R. and Hall,I.M. (2010) BEDTools: a flexible suite of utilities for comparing genomic features. *Bioinformatics*, **26**, 841–842.
35. Bailey,T.L., Johnson,J., Grant,C.E. and Noble,W.S. (2015) The MEME Suite. *Nucleic Acids Res.*, **43**, W39–W49.
36. Hagemann,S., Misiak,D., Bell,J.L., Fuchs,T., Lederer,M.I., Bley,N., Hammerle,M., Ghazy,E., Sippl,W., Schulte,J.H., *et al.* (2023) IGF2BP1 induces neuroblastoma via a druggable feedforward loop with MYCN promoting 17q oncogene expression. *Mol. Cancer*, **22**, 88.
37. Jumper,J., Evans,R., Pritzel,A., Green,T., Figurnov,M., Ronneberger,O., Tunyasuvunakool,K., Bates,R., Zidek,A., Potapenko,A., *et al.* (2021) Highly accurate protein structure prediction with AlphaFold. *Nature*, **596**, 583–589.
38. Ramjaun,A.R., Tomlinson,S., Eddaoudi,A. and Downward,J. (2007) Upregulation of two BH3-only proteins, bmf and bim, during TGF beta-induced apoptosis. *Oncogene*, **26**, 970–981.
39. David,C.J., Huang,Y.H., Chen,M., Su,J., Zou,Y., Bardeesy,N., Iacobuzio-Donahue,C.A. and Massague,J. (2016) TGF-beta tumor suppression through a lethal EMT. *Cell*, **164**, 1015–1030.
40. Cui,J. and Placzek,W.J. (2018) PTBP1 enhances miR-101-guided AGO2 targeting to MCL1 and promotes miR-101-induced apoptosis. *Cell Death. Dis.*, **9**, 552.
41. Gregory,P.A., Bracken,C.P., Smith,E., Bert,A.G., Wright,J.A., Roslan,S., Morris,M., Wyatt,L., Farshid,G., Lim,Y.Y., *et al.* (2011) An autocrine TGF-beta/ZEB/miR-200 signaling network regulates establishment and maintenance of epithelial-mesenchymal transition. *Mol. Biol. Cell*, **22**, 1686–1698.
42. Braun,J., Hoang-Vu,C., Dralle,H. and Huttelmaier,S. (2010) Downregulation of microRNAs directs the EMT and invasive potential of anaplastic thyroid carcinomas. *Oncogene*, **29**, 4237–4244.
43. Van Nostrand,E.L., Freese,P., Pratt,G.A., Wang,X., Wei,X., Xiao,R., Blue,S.M., Chen,J.Y., Cody,N.A.L., Dominguez,D., *et al.* (2020) A large-scale binding and functional map of human RNA-binding proteins. *Nature*, **583**, 711–719.
44. de Oliveira Freitas Machado,C., Schafranek,M., Bruggemann,M., Hernandez Canas,M.C., Keller,M., Di Liddo,A., Brezski,A., Blumel,N., Arnold,B., Bremm,A., *et al.* (2023) Poison cassette exon splicing of SRSF6 regulates nuclear speckle dispersal and the response to hypoxia. *Nucleic Acids Res.*, **51**, 870–890.
45. Treiber,T., Treiber,N. and Meister,G. (2019) Regulation of microRNA biogenesis and its crosstalk with other cellular pathways. *Nat. Rev. Mol. Cell Biol.*, **20**, 5–20.
46. Jonas,S. and Izaurralde,E. (2015) Towards a molecular understanding of microRNA-mediated gene silencing. *Nat. Rev. Genet.*, **16**, 421–433.

47. Lazzaretti,D., Tournier,I. and Izaurralde,E. (2009) The C-terminal domains of human TNRC6A, TNRC6B, and TNRC6C silence bound transcripts independently of Argonaute proteins. *RNA*, **15**, 1059–1066.
48. Brabletz,S., Schuhwerk,H., Brabletz,T. and Stemmler,M.P. (2021) Dynamic EMT: a multi-tool for tumor progression. *EMBO J.*, **40**, e108647.
49. Briskin,D., Wang,P.Y. and Bartel,D.P. (2020) The biochemical basis for the cooperative action of microRNAs. *Proc. Natl. Acad. Sci. U.S.A.*, **117**, 17764–17774.
50. Collart,M.A. (2016) The Ccr4-not complex is a key regulator of eukaryotic gene expression. *Wiley Interdiscip. Rev. RNA*, **7**, 438–454.
51. Raisch,T., Chang,C.T., Levdansky,Y., Muthukumar,S., Raunser,S. and Valkov,E. (2019) Reconstitution of recombinant human CCR4-NOT reveals molecular insights into regulated deadenylation. *Nat. Commun.*, **10**, 3173.
52. Brannan,K.W., Chaim,I.A., Marina,R.J., Yee,B.A., Kofman,E.R., Lorenz,D.A., Jagannatha,P., Dong,K.D., Madrigal,A.A., Underwood,J.G., *et al.* (2021) Robust single-cell discovery of RNA targets of RNA-binding proteins and ribosomes. *Nat. Methods*, **18**, 507–519.
53. Chen,H., Li,Y., Zhang,J., Ran,Y., Wei,J., Yang,Y. and Shu,H.B. (2013) RAVER1 is a coactivator of MDA5-mediated cellular antiviral response. *J. Mol. Cell Biol.*, **5**, 111–119.
54. Fink-Baldauf,I.M., Stuart,W.D., Brewington,J.J., Guo,M. and Maeda,Y. (2022) CRISPRi links COVID-19 GWAS loci to LZTFL1 and RAVER1. *EBioMedicine*, **75**, 103806.

Received: June 15, 2023. **Revised:** December 24, 2023. **Editorial Decision:** January 9, 2024. **Accepted:** January 12, 2024